SolarDynamics

Final Technical Report for Public Release

DE-EE0008140: SMART: Simplified Melting And Rotation-joint Technology

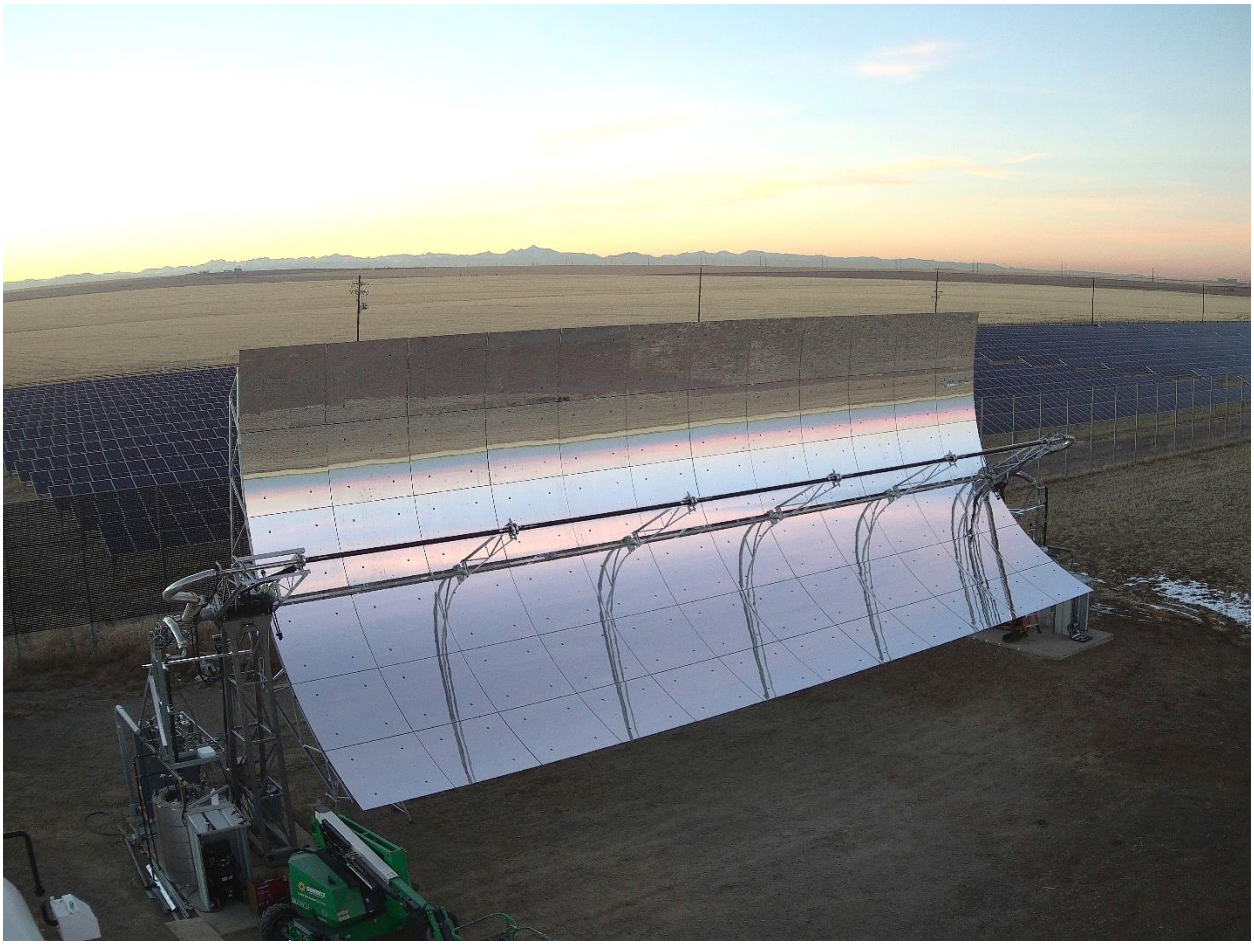

Prepared by:

Solar Dynamics, L.L.C. 1105 W. 11th Ct., Broomfield, CO, USA 80020

Revisions			
Rev	Description	By	Date
0	For public release	R. Shininger	17 November 2021
1	Removed patent notice p1, corrected reference p62	R. Shininger	18 August 2022

Project Title:	SMART: Simplified Melting And Rotation-joint Technology
Project Period:	10/01/2017 – 06/30/2021
Reporting Period:	10/01/2017 – 06/30/2021
Submission Date:	11/17/2021
Award Budget:	$2,184,672
Federal Share:	$1,710,263
Recipient Share:	$474,409
Recipient:	Solar Dynamics, LLC
Address:	1105 W. 11th Ct.
	Broomfield, CO 80020
Website:	https://www.solardynllc.com/
Award Number:	DE-EE0008140
Project Team:	Solar Dynamics, LLC
Principal Investigator:	Ryan Shininger, Senior Engineer
	Phone: +1-720-308-0744
	Email: ryan.shininger@solardynllc.com
Business Contact:	Hank Price, Managing Director
	Phone: +1-720-955-6404
	Email: hank.price@solardynllc.com
Project Partners:	NREL, Guangdong Zhu Madison Scientific, Mark Anderson Advisian, Ryan Bowers Virtual Mechanics, Juan Valverde Huiyin Group, Juha Ven Senior Flexonics, Francisco Ortiz Vives Brayton Energy, Bill Caruso
HQ Tech Manager:	David Walter
HQ Project Officer:	Jeremey Mikrut
GO Grant Specialist:	Edward Campbell
GO Contracting Officer	Diana Bobo

This material is based upon work supported by the U.S. Department of Energy's Office of Energy Efficiency and Renewable Energy (EERE) under the Solar Energy Technology Office Award Number DE-EE0008140.

Acknowledgement:

This material is based upon work supported by the U.S. Department of Energy's Office of Energy Efficiency and Renewable Energy (EERE) under the Solar Energy Technology Office (SETO), SunShot Technology to Market Award Number DE-EE0008140.

Disclaimer:

This report was prepared as an account of work sponsored by an agency of the United States Government. Neither the United States Government nor any agency thereof, nor any of their employees, makes any warranty, express or implied, or assumes any legal liability or responsibility for the accuracy, completeness, or usefulness of any information, apparatus, product, or process disclosed, or represents that its use would not infringe privately owned rights. Reference herein to any specific commercial product, process, or service by trade name, trademark, manufacturer, or otherwise does not necessarily constitute or imply its endorsement, recommendation, or favoring by the United States Government or any agency thereof. The views and opinions of authors expressed herein do not necessarily state or reflect those of the United States Government or any agency thereof.

Table of Contents

This material is based upon work supported by the U.S. Department of Energy's Office of Energy Efficiency and Renewable Energy (EERE) under the Solar Energy Technology Office Award Number DE-EE0008140.

This material is based upon work supported by the U.S. Department of Energy's Office of Energy Efficiency and Renewable Energy (EERE) under the Solar Energy Technology Office Award Number DE-EE0008140.

1 Foreword

This work was prepared under U.S. Department of Energy contract No. DE-EE0008140 resulting from Funding Opportunity Announcement DE-FOA-0001640. The project was awarded and launched in October 2017. The Budget Period 1 continuation meeting was held on February 28, 2019 and a second Budget Period was later approved. The project concluded in June, 2021.

A number of Solar Dynamics team members and contractors made significant contributions to the project, including:

> Luca Imponenti, Ryan Shininger, Keith Gawlik, Kyle Kattke, Kangqian Wu, Nathan Stegall, Rick Sommers, Tim Wendelin, Patrick Marcotte, Hank Price, Madison Scientific (subrecipient), the National Renewable Energy Laboratory (NREL), Senior Flexonics (subrecipient), Brayton Energy, Huiyin, Advisian (WorleyParsons Group, subrecipient), and Virtual Mechanics (Virtualmech, subrecipient).

Testing activities were conducted at the Solar Technology Acceleration Center (SolarTAC) in Watkins, Colorado in addition to the University of Wisconsin-Madison. Solar Dynamics would like to thank Huiyin Group for contributing the HCEs used for outdoor testing at the SolarTAC test site.

This material is based upon work supported by the U.S. Department of Energy's Office of Energy Efficiency and Renewable Energy (EERE) under the Solar Energy Technology Office Award Number DE-EE0008140.

2 Definitions & Abbreviations

CFD	Computational Fluid Dynamics
CSP	Concentrating Solar Power
DOE	U.S. Department of Energy
FEA	Finite Element Analysis
HCE	Heat Collection Element (the evacuated receiver tube assembly)
HTF	Heat Transfer Fluid
LCOE	Levelized Cost of Electricity
MS	Molten Salt
SCA	Solar Collector Assembly; a row of 8-12 SCEs linked to a central drive actuator
SCE	Solar Collector Element; a single concentrator module (1 frame + mirrors + HCEs)
SD	Solar Dynamics LLC
SunBeam™	Trade name adopted by Solar Dynamics for the new space frame technology
TRL	Technology Readiness Level, evaluated according to EERE guideline [1]

This material is based upon work supported by the U.S. Department of Energy's Office of Energy Efficiency and Renewable Energy (EERE) under the Solar Energy Technology Office Award Number DE-EE0008140.

3 Executive Summary

Oil based parabolic trough solar power plants are the most commercially mature CSP technology. However, the upper limit of about 400°C of the current organic heat transfer fluid (HTF) significantly limits the future potential of the technology. Advances in parabolic trough receiver and collector technology have enabled higher operating temperatures of potentially 500°C or above. The search for an improved higher temperature HTF has identified inorganic molten salts, specifically the mix referred to as Solar Salt, a 60:40 mix of sodium nitrate and potassium nitrate salt. However, Solar Salt starts to freeze at about 240°C. This poses a significant challenge for large parabolic trough plants that could have many kilometers of header piping and hundreds of kilometers of receiver piping, all filled with molten salt. Plants using molten salt need to be designed to minimize the risk of freezing and to be able to recover from freeze events. Studies and field experiments have shown that this appears to be feasible, and the approach appears to have strong economic advantages over conventional trough plants. However, some technical challenges remain related to the use of molten salt in trough solar fields, the cost of the freeze recovery system is significant, and many still question whether the risk of using molten salt is worth the economic upside. In our view, the potential economic upside justifies the continued look at molten salt HTF in parabolic trough plants.

The objective of this project was to address the key technical issue remaining, look for opportunities to reduce the cost of the freeze recovery system, and improve the general information and tools available for assessing the design, performance and economics of trough plants using molten salt HTF.

- Freeze-protection systems may add \$80/m^2 or more to the solar field cost. Most of this cost is attributed to receiver heating. We developed approaches that significantly reduce the cost of freeze protection and freeze recovery to less than \$10/m^2. We conducted field testing to help validate these concepts.
- No collector interconnect had demonstrated a 10-year interconnect service life in molten salt which is the minimum that would be considered commercially reasonable. We demonstrated a commercial solution that achieved a 30-year simulated life under laboratory cyclic testing at operating temperatures and pressures.
- Most parabolic trough simulation models were inadequate to support development and stakeholder review of a plant conceptual engineering designs using molten salt HTF. Working with NREL, we adapted the NREL System Advisor Model to simulate a molten-salt trough plant more accurately. Working with Advisian, we developed an updated cost model that works with SAM to allow accurate comparisons between oil and molten salt trough plant configurations.
- We modeled two reference-plant configurations to evaluate the benefit of molten salt HTF in parabolic trough plants. The first was what we refer to as a peaker plant designed to meet a peak load between 4pm and 10pm during summer months. The second was a baseload configuration. In both cases, the molten-salt HTF results in major cost reductions for parabolic trough plants. If these cost reductions can be achieved in practice, it makes parabolic trough technology very competitive with molten-salt tower technology.
- Finally, we identify some of the next steps of development for molten salt HTF in tough plants. These include further development and testing of interconnects and the solar field freeze recovery system, and then moving to full scale field testing.

This material is based upon work supported by the U.S. Department of Energy's Office of Energy Efficiency and Renewable Energy (EERE) under the Solar Energy Technology Office Award Number DE-EE0008140.

4 Motivation

The use of molten salts as the heat transfer fluid (HTF) in parabolic trough collectors was first studied by Kearney & Associates [2]. The motivation for doing so is the higher operating temperature, raising the peak operating temperature of trough plants from about 400°C to 550°C or above, and associated higher Rankine cycle efficiencies and lower cost Thermal Energy Storage Systems (TES). The main concern with using molten salt in a trough solar field is the high freeze point. Solar Salt, a 60/40 mix by weight of $NaNO_3/KNO_3$, is one of the preferred mixtures; which freezes over a range of temperatures, approximately 220 – 240°C. The Kearney & Associates study determined the concept was feasible and identified several key issues needed to commercialize the technology:

- A significant challenge is the simplification and cost reduction of the heat tracing and the sealing of ball joints or alternative rotation joints.
- Development of a high temperature selective coating for trough receivers is needed.
- Prototype testing of components and salt HTF loop testing would be required.

ENEA, the Italian Research Laboratory, was one of the first to test many components and operated a full-scale collector test loop with molten salt [3]. They demonstrated the feasibility of using solar salt at up to 565°C as the HTF in a trough collector field, as well as using impedance heating for freeze protection and daily drain back of the loop for freeze protection. They also demonstrated it was possible to recover from a freeze event.

Archimedes Solar and Schott Solar both developed high temperature receivers and selective coatings optimized for use with molten-salt up to 565°C.

Abengoa Solar studied the use of molten-salt HTF and found that molten-salt clearly holds cost advantages, however no collector interconnection solution was found that would survive for a 30-year commercial life [4].

Freeze recovery and protection has been demonstrated with electrical heating systems [5] [6]. Although this appears to be a good technical solution for heating, it is not cost effective and challenging to scale for commercial plants [7]. Finally, only limited information is available on past tests and demonstration projects.

This project was launched to directly tackle the most critical technical challenges: the freeze-recovery subsystem, the rotation-expansion piping joints that connect the collector receivers to the header piping, and the optimization of the standard collector loop and solar field arrangements based on recent hardware innovations.

This material is based upon work supported by the U.S. Department of Energy's Office of Energy Efficiency and Renewable Energy (EERE) under the Solar Energy Technology Office Award Number DE-EE0008140.

5 Interconnect Technologies & Testing

A significant barrier to commercializing the use of molten salt in trough plants is the lack of a reliable collector interconnect, also known as “REPA” (Rotation Expansion Performing Assemblies). In a CSP solar field, interconnects are located on either end of the collector and allow the necessary degrees of freedom between the receiver tubes and the fixed process piping: revolution about the collector axis and linear thermal expansion of the receiver tubes. The most used interconnects in commercial trough plants operating with organic HTF are ball joint assemblies as shown in Figure 1.

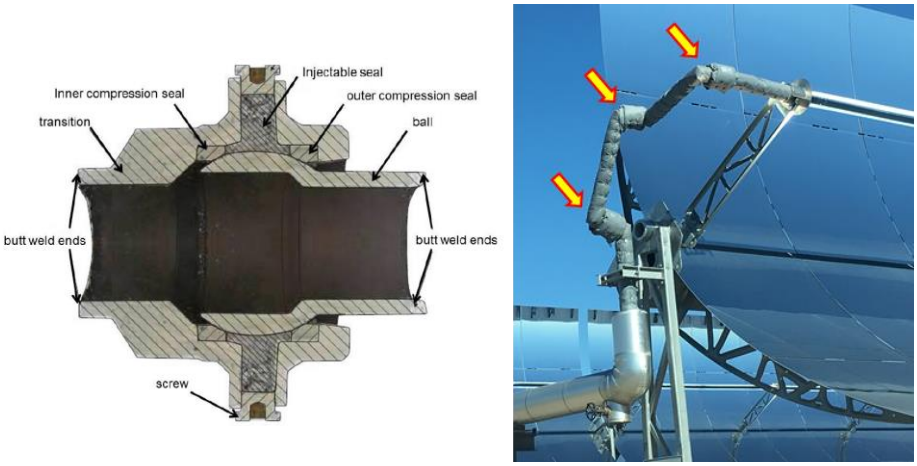

Figure 1. Ball joint (left) and ball joint assembly installed at Genesis Solar Energy Project (right)

However, these ball joints contain an injectable packing material containing graphite which rapidly oxidizes when exposed to nitrate salts at elevated temperatures [8]. Previously, Abengoa Solar tested more than 13 different variations of ball joint and rotary joint designs with limited success [4].

A second type of interconnect used in the earliest commercial trough plants are flexible hoses or “flex hoses.” Early flex hose designs suffered from significant pressure drops from fluid constriction, under-constrained geometry, and quality control issues. Later installations have incorporated rotary joint to accommodate the rotation requirements, thereby constraining the movement of the flexible hose for thermal expansion of the receiver only.

Figure 2. LS-2 Flex Hose at SEGS III (left) and flex hose assembly with rotary joint at Mojave Solar Project (right)

This material is based upon work supported by the U.S. Department of Energy’s Office of Energy Efficiency and Renewable Energy (EERE) under the Solar Energy Technology Office Award Number DE-EE0008140.

A commercially viable collector interconnect had never been fully validated for molten salt service. This project aimed to evaluate two new collector interconnect options, 1) a new flexible hose interconnect assembly designed by Senior Flexonics, the RotationFlex Triple System, or "RF-Triple®", and the Brayton Energy Flexible Rotary Pipe Coupler.

5.1 Interconnect Design – RotationFlex Triple System

Senior Flexonics' RotationFlex Triple System was designed based on a few principles; fatigue life for flexible hoses can be maximized when the motion of a flex hose can be constrained to 1) bend in a single plane, 2) bend in only one direction, never reversing in the opposite direction, and 3) limit the degree of bending. The RF-Triple® system contains three separate hoses to accommodate the motion of the CSP collector; one hose to accommodate the axial motion from HCE thermal expansion, and two hoses to split the duty of the 180° rotational need, each bending from 0° to 90°. The main advantages are: 1) the whole system is contained without the use of any sealing surfaces, 2) it is suitable for electrical resistive heating, and 3) the system includes a special insulation which also serves as outer mechanical protection. This configuration is depicted in Figure 3.

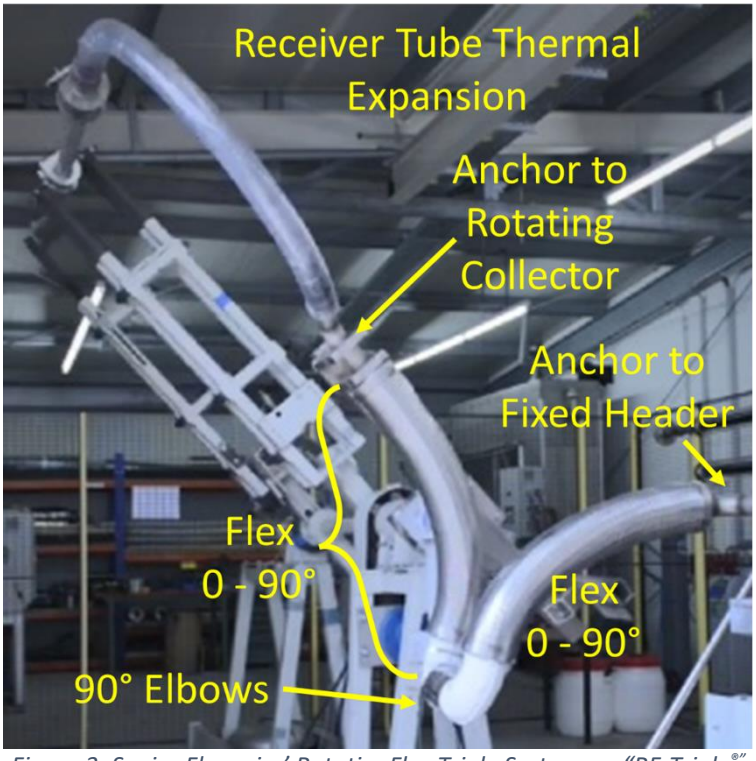

Figure 3: Senior Flexonics' RotationFlex Triple System, or "RF-Triple®".

There are also some notable disadvantages of this design compared to oil-based system designs including: 1) higher expense, 2) greater complexity of installation, 3) insulation at the interfaces between subcomponents can cause cold spots at low mass flow rates, and 4) limited operational experience.

This material is based upon work supported by the U.S. Department of Energy's Office of Energy Efficiency and Renewable Energy (EERE) under the Solar Energy Technology Office Award Number DE-EE0008140.

5.2 Interconnect Design – Flexible Rotary Pipe Coupler

An alternative and novel interconnect design is the Brayton Energy flexible rotary pipe coupler, a continuous pipe wound into a helix, allowing large angular and axial displacements with modest stress, and functioning on the same principle as a mechanical spring.

This design was studied in detail and reported by Brayton Energy in a separate DOE-funded project, Award # DE-SC0011965 [9]. The design eliminates seals, thin-walled bellows, and highly stressed small radius convolutions. The primary risk to the design is achieving required flexibility in a compact cost-competitive package. Use of standardized components and readily available materials reduces the total cost, budgetary uncertainty, and allows for a competitive supply chain.

Brayton Energy designed the interconnect solution for use with molten salt, constructed and tested a full-scale prototype in a lab, and concluded that the concept is technically feasible. Furthermore, they recommended further systems-level power plant optimization to compare the performance considering hydraulic head losses, energy losses, and lifecycle O&M costs. Solar Dynamics undertook this effort in Budget Period 1, subcontracting Brayton Energy to adapt their design to the geometry of the Solar Dynamics SunBeam™ collector (the parabolic trough system developed under the "ATLAS" contract [10]) and use the resulting information to perform systems analysis compared to a flex hose design.

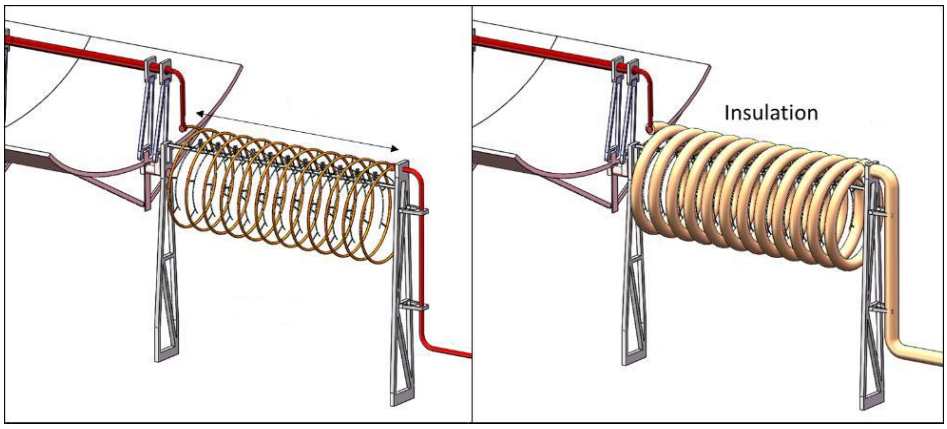

Figure 4. Brayton Energy Flexible Rotary Pipe Coupler design

This design presents certain advantages and disadvantages over ball joints and flex hoses, as summarized below:

Advantages:

- Robust sealing - continuously welded system allows little opportunity for leaks
- Components are widely available, relatively easy to fabricate

Disadvantages:

- Increased head losses due to substantial additional pipe length
- Increased heat losses due to large surface area of piping
- Increased land consumption
- Difficult to drain for maintenance
- Higher unit cost

This material is based upon work supported by the U.S. Department of Energy's Office of Energy Efficiency and Renewable Energy (EERE) under the Solar Energy Technology Office Award Number DE-EE0008140.

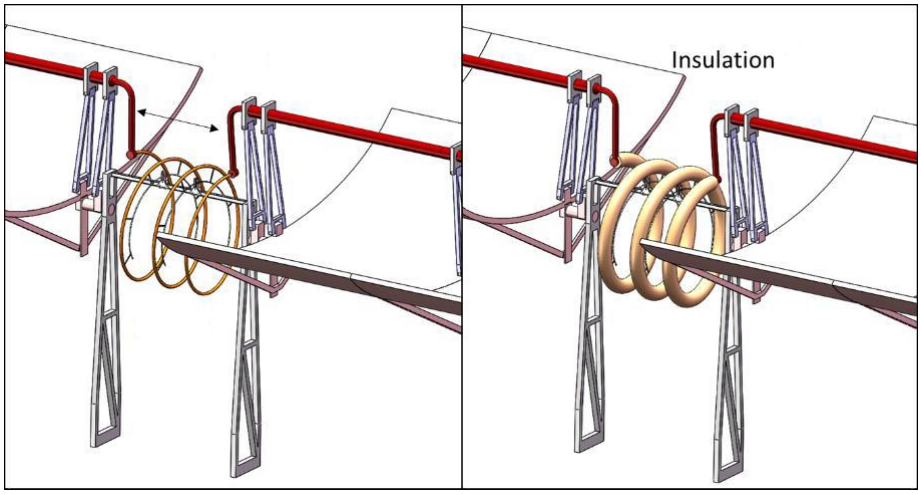

Figure 5. Brayton Energy Flexible Rotary Pipe Coupler design for collector-to-collector interconnect

Solar Dynamics conducted a techno-economic analysis of the flexible rotary pipe coupler design compared to the TripleFlex triple flex hose design and ultimately determined to pursue a flex hose design. This analysis is covered in detail in section 11.9.1.

5.3 Interconnect Testing – Description & Results

Two interconnect designs were considered for use with molten salt in this study, the Senior Flexonics TripleFlex flex hose solution and the Brayton Energy flexible rotary pipe coupler. A systems study identified that the flex hose solution appeared to provide the best overall solution if it could demonstrate a reasonable lifetime, in this case a minimum 10-year service life without failure. A test rig was designed and constructed by Professor Mark Anderson of Madison Scientific at the University of Wisconsin, Madison to mechanically cycle the RotationFlex Triple interconnect according to its daily commercial use with molten salt at temperatures and pressures representing the commercial operating conditions (300°C at 32 bar and 550°C at 14 bar). The test rig is shown in Figure 6 and Figure 7.

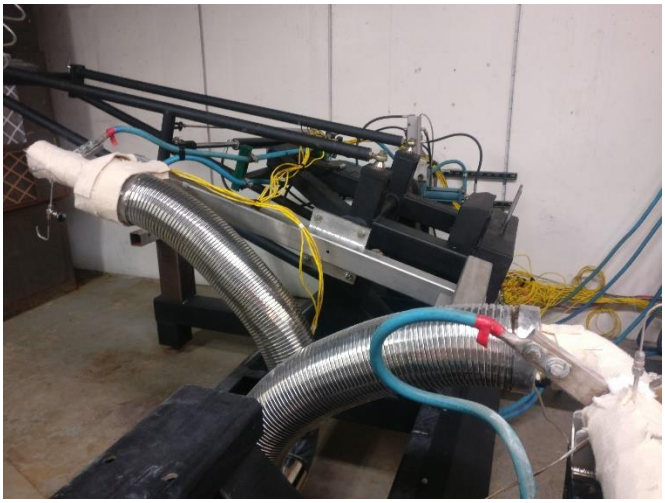

Figure 6: RF-Triple™ without Receiver tube thermal expansion component, extended to nearly 180° rotation

This material is based upon work supported by the U.S. Department of Energy's Office of Energy Efficiency and Renewable Energy (EERE) under the Solar Energy Technology Office Award Number DE-EE0008140.

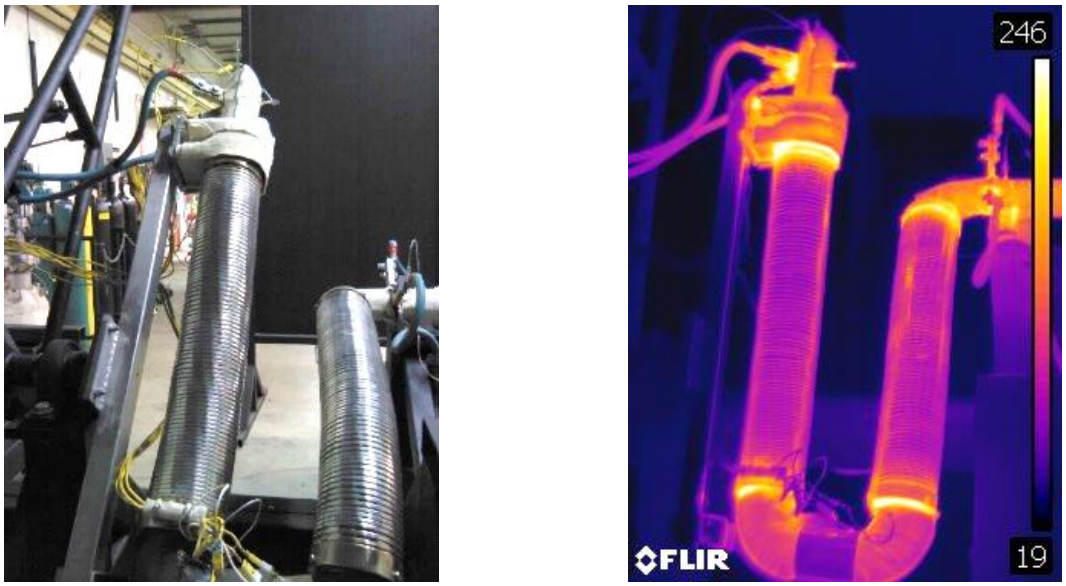

(a) (b)

Figure 7: Images of the RF-Triple®: (a) installation without Receiver thermal expansion component on test bench by Madison Scientific at the University of Wisconsin, and (b) high temperature, high pressure IR image at 550 °C.

The rig was fully instrumented for torque, temperature, pressure, and salt level measurements. The test conditions are listed in Table 1 below.

*Table **1**. Interconnect test conditions*

	Test 1: Outlet conditions	**Test 2: Inlet conditions**
Fluid	Solar Salt (60% $NaNO_3$, 40% KNO_3)	
Pressure	14.0 bar	31.5 bar
Temperature	550 °C	305 °C
Rotation	0° to 180° tracking angles (horizon to horizon)	
Cycle Frequency	2 minutes per cycle	
Success Criteria	3,600 cycles, representing 10 years of service	
Results	11,000+ cycles completed without failure, representing 30+ years	10,200+ cycles completed, representing 28 years of service

A deconstructive postmortem analysis of the flex hose of Test 2 concluded that a small crack formed as a result of fatigue, as expected according to the quantity of cycles under which it was subjected.

The successful test results demonstrated acceptable performance under the most challenging conditions expected during operation with respect to pressure, temperature, and fatigue life of the Senior Flexonics' RF-Triple® design in a molten salt parabolic trough CSP collector. Although these are accelerated tests which lack corrosion, temperature cycling, and other long term in-field effects, the results are promising and suggest a unique, economically viable solution for molten salt trough systems.

This material is based upon work supported by the U.S. Department of Energy's Office of Energy Efficiency and Renewable Energy (EERE) under the Solar Energy Technology Office Award Number DE-EE0008140.

6 Thermal-fluid and Mechanical Modeling of HCE Freeze Recovery

Given the high freeze point for molten salt (~ 240°C for Solar Salt), it is reasonable to assume that a plant using molten salt as the HTF will experience some freeze events in the solar field over its lifetime. This could range from single loops of collectors to full subfields. It is essential that the solar field be designed to recover from freeze events. Various strategies have been considered for avoiding freezing and or recovering from freezing. Prior studies have identified that impedance (Joule effect) heating, i.e., resistive heating of a component by applying an electrical current, can be used to heat the receiver tubes in the solar field [7] [8] [4]. However, challenges with full-scale implementation [7] and high costs [4] raise doubts regarding the commercial viability of such a system and generate motivation for the development of alternative heating systems. Joule Heating is the process by which the passage of an electric current through a conductor produces heat. The term “impedance heating” implies the use of alternating current, which in addition to the Joule Heating effect, also results in additional heating from the “skin effect” and the “hysteresis effect” [11]. Noting these technical differences, the terms “Joule Heating” and “impedance heating” are often used interchangeably in the CSP industry and are also used interchangeably in this report.

To better understand the melting process, it is important to be able to model the freeze recovery of receivers in the solar field. This focuses both on the sizing of the Joule heating system required to thaw a frozen loop of collectors in the desired time, and to understand the mechanical stress imposed on the receivers during freeze/thaw events. This section discusses the modeling efforts undertaken in this project to evaluate the HCE integrity through salt melting and looks at the potential to use solar-assisted freeze recovery.

6.1 Model description

In Budget Period 1 (BP1) a 2D constant density model of the HCE was developed in collaboration with NREL and used to evaluate the feasibility of solar heating for freeze recovery[1]. Results from this model indicated solar heating was possible if the circumferential ΔT across the receiver tube was maintained below 72°C, this corresponds to a minimum melt time of about 5.5 h at 1000 W/m^2 DNI (with a direct incidence angle). These initial modeling efforts are described in detail in a peer reviewed publication [12]. The encouraging results of the proof-of-concept modeling in BP1 lead to further model development in BP2 with the following improvements: a more complex 3D domain and updated salt thermophysical properties to capture variations with temperature. Details of this updated model can also be found in [13], a summary is provided in this section. The modeling work described in this section was performed by Virtualmech unless otherwise noted. The two models can be referred to as the “conduction” and “natural convection” models, for the constant density and temperature-dependent density functions, respectively, based on the dominant mode of heat transfer in each case.

Due to the significant computational resources required to solve a 3D thermal-fluid model of the melting process, a typical HCE is assumed to be symmetrical in the axial direction. Half of an HCE is modelled with symmetry boundary conditions on both the bellows and the center of the HCE. For the fluid domains there are no-slip conditions at the inner absorber tube surface, as well as the outer absorber

[1] NREL work funded under DE-AC36-08GO28308 in support of this project.

This material is based upon work supported by the U.S. Department of Energy’s Office of Energy Efficiency and Renewable Energy (EERE) under the Solar Energy Technology Office Award Number DE-EE0008140.

surface and inner glass envelope wall. Thermal boundary conditions include radiative and convective heat losses from both absorber and glass surfaces, as well as the relevant heat source at the absorber wall which will be described in detail in the following sections. The receiver wall temperature is monitored with 6 circumferential temperature probes at 3 axial locations (center of bellows, bellows-HCE interface, center of HCE). The mesh for solid and fluid domains is illustrated in Figure 8 (a) and (b), respectively. The solid domain includes the bellows and glass envelope as shown by the cross-sectional cut in Figure 8 (a), this is meant to better visualize the mesh detail as the full circumference is ultimately modelled.

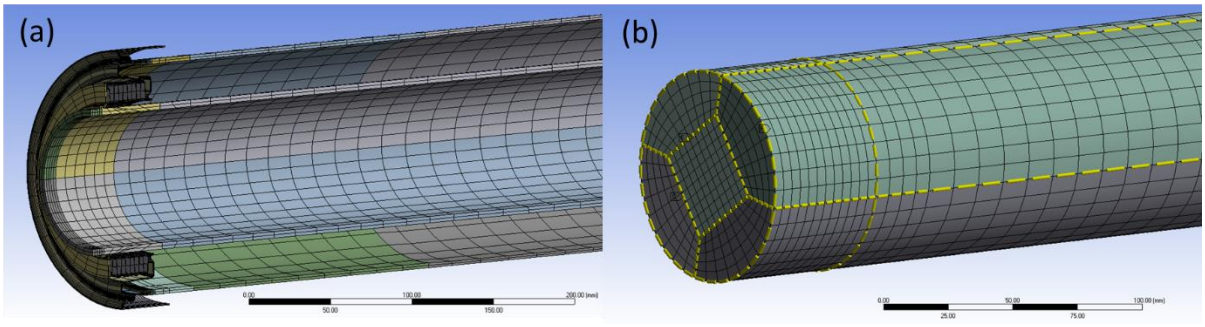

Figure 8: Updated mesh for (a) solid and (b) fluid domains. The axial variations in element size helped with numberical stability in the natural convection model..

In addition to developing the thermal-fluid model for the thaw process, Virtualmech also developed a mechanical finite element (FE) model to evaluate stresses and identify the most common failure modes for a string of HCEs. This task was accomplished using a different model of salt flowing through the receiver tubes, i.e., salt flow model, which does not include solidification and melting source terms. Modeling a string of four HCEs is ideal for accurate stress results, but this domain is very large to couple with the computationally expensive thermal-fluid model required for the thaw process. The salt flow model coupled with an FEA solver was used to identify the weakest point in a string of 4 HCEs. Results indicate the maximum deflection of any given HCE always occurs in the middle cross-section and the maximum stress points are either at the outlet of the HCE string or at one of the welded interconnects. Therefore, the most common failure modes include contact of absorber tube with the glass envelope at the center of the HCE, or high stresses at the HCE connections. This study was the basis for developing an FE model of a 2 HCE string to evaluate the integrity of the HCE during a freeze recovery event. The reduced computational domain yields values for maximum deflection and von Mises stress within 2.3% of the ideal 4 HCE string solution, as shown by the results in Table 2.

Table 2: Comparison of the maximum deflection and Von Mises stress observed in simulations with varying number of HCEs in the computational domain.

# of HCEs	Max. Deflection [mm]	% Difference Deflection	Max. von Mises Stress [MPa]	% Difference Stress
4	12.10	0	147.67	0.00
2	11.82	2.29	145.00	1.81

This material is based upon work supported by the U.S. Department of Energy's Office of Energy Efficiency and Renewable Energy (EERE) under the Solar Energy Technology Office Award Number DE-EE0008140.

To evaluate the HCE integrity during freeze recovery, the thermal-fluid model solves for the temperature profile of half an HCE with symmetry conditions at the bellows and center of the HCE. Taking advantage of these symmetry conditions, and assuming the adjacent HCE also has a symmetry condition at the center of the illuminated length, results in 2 full HCEs with the same temperature profile. In this work, the temperature profile with the highest thermal gradients output from the thermal-fluid model is extrapolated to 2 HCEs for a static structural analysis.

For this component two different types of heating are considered: an electrically powered system based on Joule heating, and solar heating from concentrated light from the collector tracking the sun. Proof-of-concept modeling work performed by Solar Dynamics and NREL in BP1 suggests that solar flux heating of the HCEs is possible if the heat is attenuated and spread around the absorber by continuously focusing and defocusing the parabolic mirrors, i.e., track-through or pass-through focus [12]. Model results for each heating method are described in the following sections.

6.1.1 Heat Transfer Fluid

The heat transfer fluid considered in these modeling efforts include Solar Salt (60% $NaNO_3$, 40% KNO_3 by weight) and air. Most simulations focused on characterizing the melting process of Solar Salt in the HCEs. Due to challenges experienced at the outdoor test site which prevented testing with salt, some simulations with air are performed for comparison to experimental data. Simulations with air only include the solid domain and an appropriate boundary condition at the inner receiver wall.

The thermophysical properties of Solar Salt in BP2 were updated to capture variations during the melting process, significantly increasing model complexity. Relevant thermophysical properties are plotted in Figure 9, including temperature-dependent density to capture buoyant forces, specific heat with an additional peak for the solid-solid phase transition, and thermal conductivity with solid phase data [14]. Furthermore Δh_f is decreased to 115520 J kg^{-1}, since the latent heat associated with the solid-solid phase transition enthalpy is captured in the specific heat function, compared to the BP1 model which used a constant c_p and higher Δh_f.

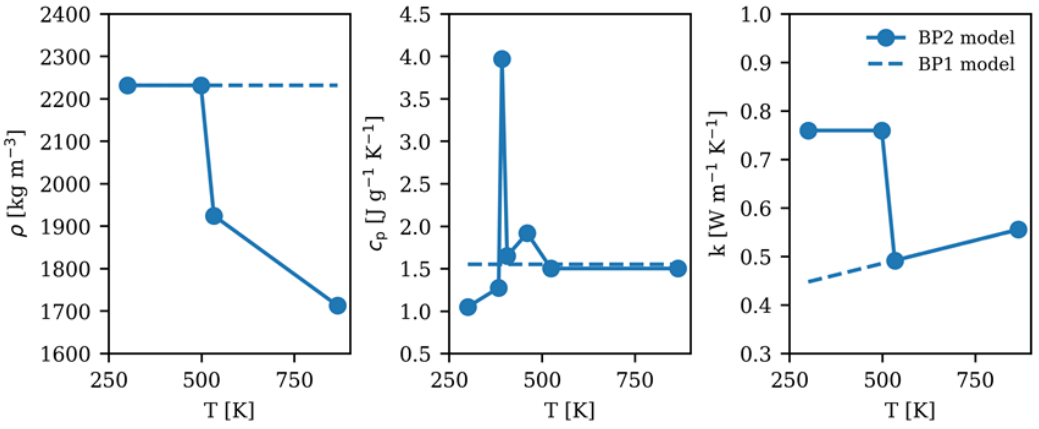

Figure 9: Thermophysical properties of Solar Salt updated in BP2 to include variations with temperature as measured in Iverson et al. 2012. (a) Density, (b) specific heat, and (c) thermal conductivity used in thermal-fluid model. The specific heat curve includes the solid-solid phase transition occurring around 120°C.

This material is based upon work supported by the U.S. Department of Energy's Office of Energy Efficiency and Renewable Energy (EERE) under the Solar Energy Technology Office Award Number DE-EE0008140.

6.2 Joule Heating

Joule heating is modelled as a spatially uniform heat flux at the outer receiver wall. One of the big advantages of this method is the uniform heat input, including non-illuminated regions of the receiver tube. This mode of heating was considered in 2D simulations of solar salt melting in the HCE with both constant density and with density variations; the resulting melt times are compared in Table 3. The natural convection simulations also capture the latent heat attributed to the solid-solid phase transition occurring around 125°C, which results in the slower onset of melting observed in Table 3. Once the salt begins to thaw, density changes result in buoyant flow and natural convection heat transfer which significantly increases heat transfer during melting. Despite the slower onset of melting, simulations with density as a function of temperature complete the melting process 2.66 h and 0.81 h faster compared to constant density simulations at 150 and 300 W m^{-1} impedance heating, respectively. These time differences highlight the importance of natural convection once the melting process begins. Based on these results it will be necessary to include natural convection in 3D models to accurately estimate melting times.

Table 3: Melt time and onset of melting for 2D thermal-fluid simulations of the thawing of Solar Salt using impedance heating with and without density variations through the phase change.

Density [kg m^{-3}]	Impedance Heat [W m^{-1}]	Onset of melting [h]	Melt time [h]
2232	150	8.82	18.51
f (T)	150	9.23	15.85
2232	300	3.79	7.51
f (T)	300	3.9	6.70

While comparisons of different models were performed in 2D, modeling efforts in 3D focused on melting simulations with natural convection. Previous design studies of molten salt parabolic trough plants considered power densities up to 250 W m^{-1} for freeze recovery of the solar field [8]. Results of the 3D HCE model with 250 W m^{-1} of Joule heating are shown in Table 3; the plotted contour captures the largest thermal gradient of the simulation which occurs when 60% of the salt has melted. In this case axial and radial gradients are minimized due to the uniform Joule heating method. The difference in heat losses between the bellows and exposed HCE results in a 12°C difference along the receiver length, with the maximum temperature occurring at the insulated interconnect. The total melt time required for this simulation was 12.0 hours, compared to 2D results of 11.2 hours for constant density and 9.7 hours with natural convection at 250 W m^{-1}. Despite the additional heat transfer associated with natural convection the 3D model takes longer to melt due to increased heat losses throughout the melting process, the bellows lose more heat at lower temperatures while the HCE losses are higher when radiative heat transfer begins to dominate.

This material is based upon work supported by the U.S. Department of Energy's Office of Energy Efficiency and Renewable Energy (EERE) under the Solar Energy Technology Office Award Number DE-EE0008140.

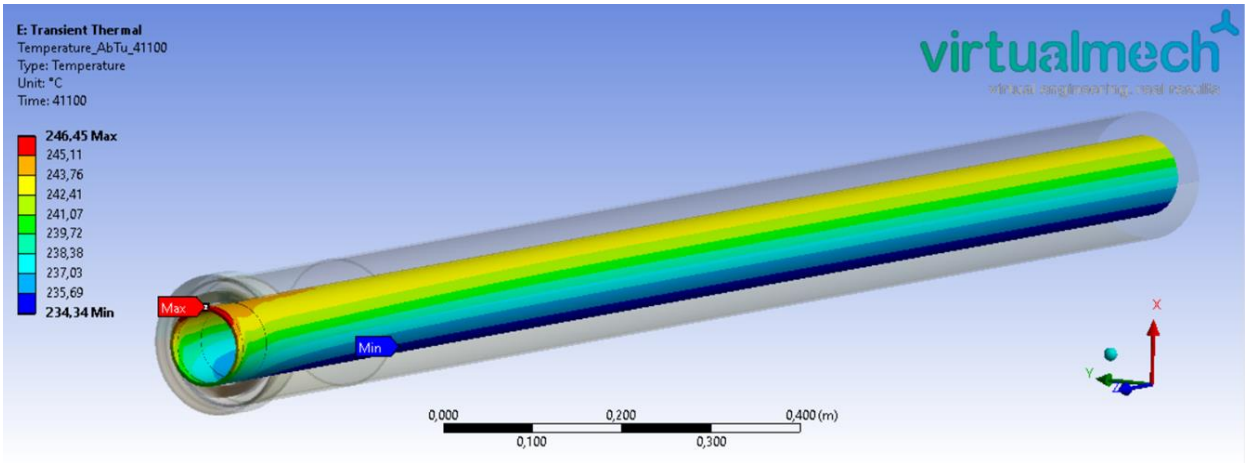

Figure 10: Temperature profile with highest thermal gradients observed during melting simulation with 250 W/m Joule heating, in this case the highest temperature occurs at the insulated interconnect.

The output of the thermal-fluid model, plotted in Figure 10, provides the input for a FEA of a two HCE string. The temperature profile with the largest thermal gradients for half the HCE is mirrored across two HCEs for the structural analysis. Results from this analysis showing the von Mises stress profiles for both the absorber tube and glass envelope are illustrated in Figure 11. Joule heating simulations indicated the maximum expected heat input of 250 W/m produced stresses that were well below the yield strength of the material for both the absorber tube (205 MPa) and the glass envelope (27 MPa). For the case of the absorber tube the maximum stress point occurs towards the center of the HCE, while the glass envelope sees the highest stresses at the joint in between the two HCEs modeled.

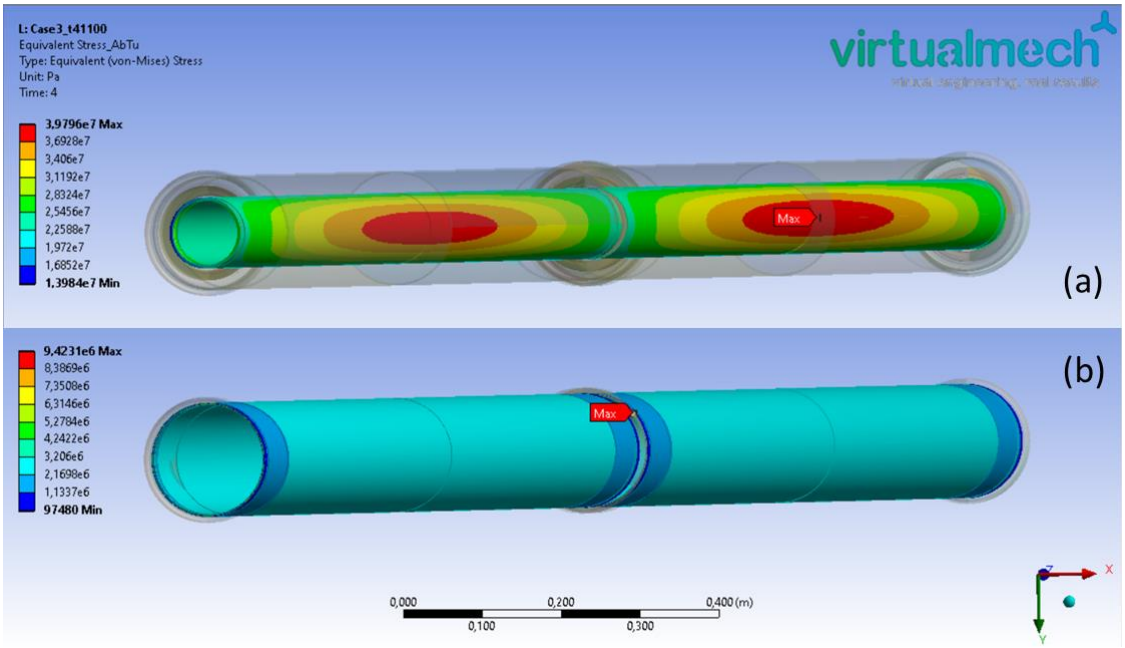

Figure 11: Results of the FEA analysis performed at the critical point of a melting simulation with 250 W/m Joule heating for (a) the absorber tube and (b) the glass envelope. In this case both components remain well under their respective yield strengths.

This material is based upon work supported by the U.S. Department of Energy's Office of Energy Efficiency and Renewable Energy (EERE) under the Solar Energy Technology Office Award Number DE-EE0008140.

Stress results for this coupled thermal-fluid-mechanical analysis assume the salt is free to expand during melting, as seen in previous freeze-thaw tests [5]. During a typical freeze recovery, salt in the headers and flexible hoses should be melted prior to solar heating of the solar field, through heat trace and Joule heating, respectively; allowing the salt in any given collector to expand in the axial direction. In a commercial system there are many factors that cause cold spots and could result in a frozen salt plug (damaged HCEs, broken mirrors, etc.), so it is possible that certain sections of the solar field experience constrained salt expansion during part of a freeze recovery event. Modeling this phenomenon is very challenging from a technical point of view, and the initial conditions after freezing are not necessarily clear in terms of void space in the receiver. For these reasons any freeze recovery system will have to be demonstrated at the relevant scale (full-size SCA or loop) before commercial application.

6.3 Solar Heating

A controllable solar flux heating method is under development to safely use concentrated solar heat from the parabolic mirrors to thaw salt frozen in the solar field. By continuously cycling the mirrors between on-focus and off-sun positions the solar heat input can be attenuated to acceptable levels for the cold temperatures expected during a freeze event. After each track-through focus the mirrors may be held off-sun for some amount of time, t_{off}, allowing heat to dissipate towards non-illuminated areas. Using this method, the flux profiles shown in Figure 12(a) generate the average solar heat flux input plotted in Figure 12(b). The heat input can be adjusted by changing the mirror rotational speed or changing the t_{off} parameter. The flux profiles in Figure 12 are specific to the SunBeam trough geometry, and will vary for different concentration ratios, rim angles, etc.; however, the solar flux heating method may be adapted to different geometries by varying the pause off-sun and/or mirror tracking speed. Initial modeling studies looked at different mirror speeds (0.1 - 0.5°/s), pauses off-sun (0 – 300 s) and the possibility of a pause on-sun (0 – 10 s) to modify the flux profile. Some important takeaways from this study are listed below:

- Faster mirror speeds are preferable to maintain lower thermal gradients.
- Slower mirror speeds require an increased t_{off}, resulting in a slower melt time to maintain HCE integrity.
- A pause on-sun is not recommended. Pausing with the mirrors on-focus can result in significant axial gradients along the collector.

Based on these results a flux profile with $t_{\text{off}} = 120$ s, a mirror speed of 0.3°/s, and no pause on-sun was selected as the starting point for 3D modeling simulations.

As a theoretical exercise a melting simulation with the full on-focus solar flux profile and no defocusing was also performed with the 3D model. This is the highest incident heat flux expected during the melting process and would normally be attenuated with the track-through method described above. Results for this simulation showing the minimum, maximum, and average receiver wall temperatures are plotted in Figure 13 (a). As expected, the thermal gradients generated in this process quickly result in receiver failure, shown in Figure 13 (b), but the thermal-fluid model is shown to be robust under challenging heating conditions. These results indicate that defocusing is necessary to safely melt salt in the receiver tube despite the heat transfer from natural convection, confirming results from the more conservative 2D conduction model.

This material is based upon work supported by the U.S. Department of Energy's Office of Energy Efficiency and Renewable Energy (EERE) under the Solar Energy Technology Office Award Number DE-EE0008140.

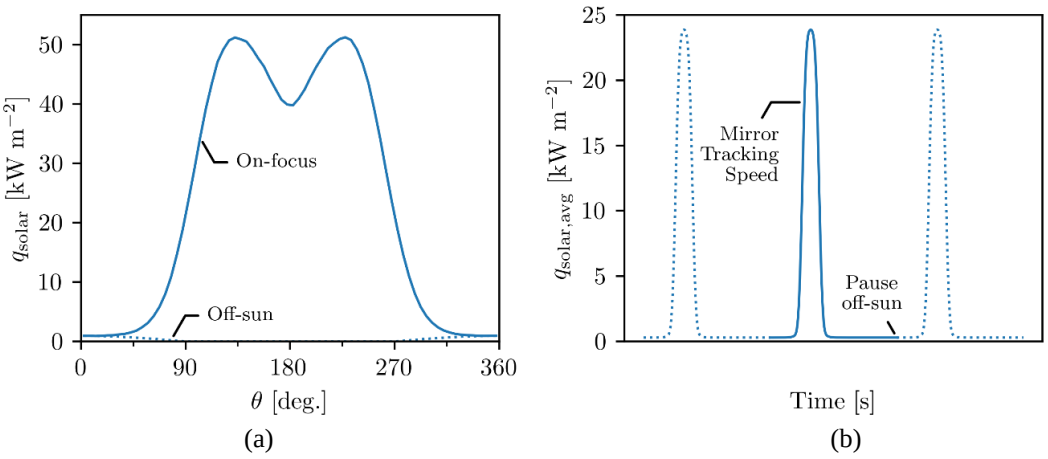

Figure 12: (a) Solar flux profile around the illuminated section of the HCE for different mirror positions, and (b) transient, spatially averaged heat flux input to HCE by rotating the mirrors between off-sun and on-focus positions

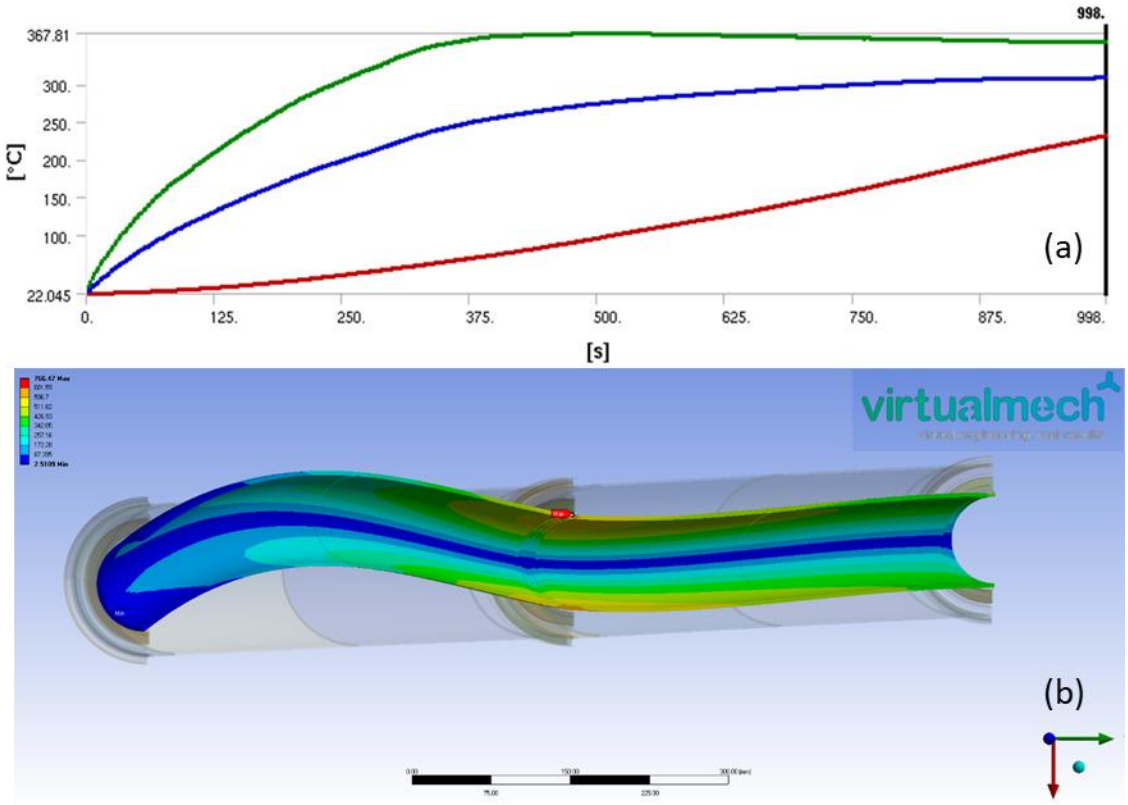

Figure 13: (a) Minimum, maximum, and average temperatures of the receiver wall during a 3D simulation for melting of Solar Salt with solar heat and no defocusing, and (b) von Mises stress profile showing the failure modes of the 2-HCE FE model.

The remaining solar heating simulations consider the track-through method for solar heating using the flux profiles in Figure 12. With the 3D model the presence of non-illuminated bellows significantly slowed down the melting process for pure solar heating compared to 2D simulations. This unheated thermal mass results in significant axial losses from the illuminated section of the HCE resulting in a melt time of 18.5 hours for $t_{\text{off}} = 120$ s. Decreasing the time off-sun to $t_{\text{off}} = 60$ s results in a melt time of

This material is based upon work supported by the U.S. Department of Energy's Office of Energy Efficiency and Renewable Energy (EERE) under the Solar Energy Technology Office Award Number DE-EE0008140.

11.9 hours while maintaining a similar maximum stress value, these results are also summarized in Table 4 The average liquid fraction in the HCEs during freeze recovery with solar heating is shown in Figure 14 the x-axis is normalized by the melt time for comparison of both solar heating simulations. The evolution of the liquid fraction is similar for both solar heating cases despite the difference in melt times. With an initial temperature of 10°C, the onset of melting occurs about halfway through the full melting process. As the liquid fraction increases past 50% there is a clear inflection point attributed to increased convection heat transfer to the remaining volume of frozen salt.

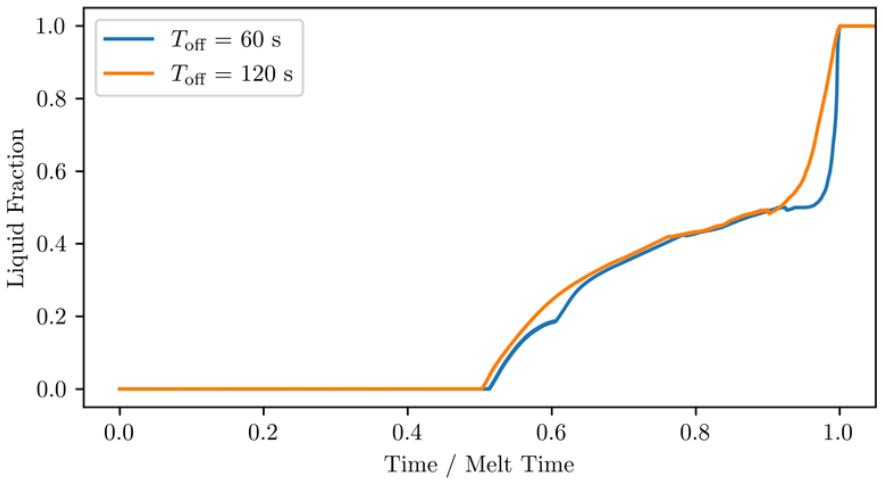

Figure 14: Evolution of the average liquid fraction in the HCEs for solar heating freeze recovery simulations from an initial temperature of 10°C.

The temperature and von Mises stress contour plots for the simulation with $t_{\text{off}} = 120$ s are plotted in Figure 15. These results are representative of the solar heating simulations with decreasing t_{off}. The hottest temperature occurs at the center of the illuminated HCE at the point closest to the mirrors, while the minimum temperature occurs at the weld between the two HCEs at the point opposite from the mirrors. The temperature profile in Figure 15(a) results in the von Mises stresses in Figure 15(b). The maximum stress value occurs at the HCE interconnect, as expected. Along the HCE length the high stress point occurs consistently on the mirror-side of the absorber tube. The temperature profile in Figure 15(a) results in a maximum radial deformation of 1.485 mm which occurs at a similar axial location as the maximum temperature value.

This material is based upon work supported by the U.S. Department of Energy's Office of Energy Efficiency and Renewable Energy (EERE) under the Solar Energy Technology Office Award Number DE-EE0008140.

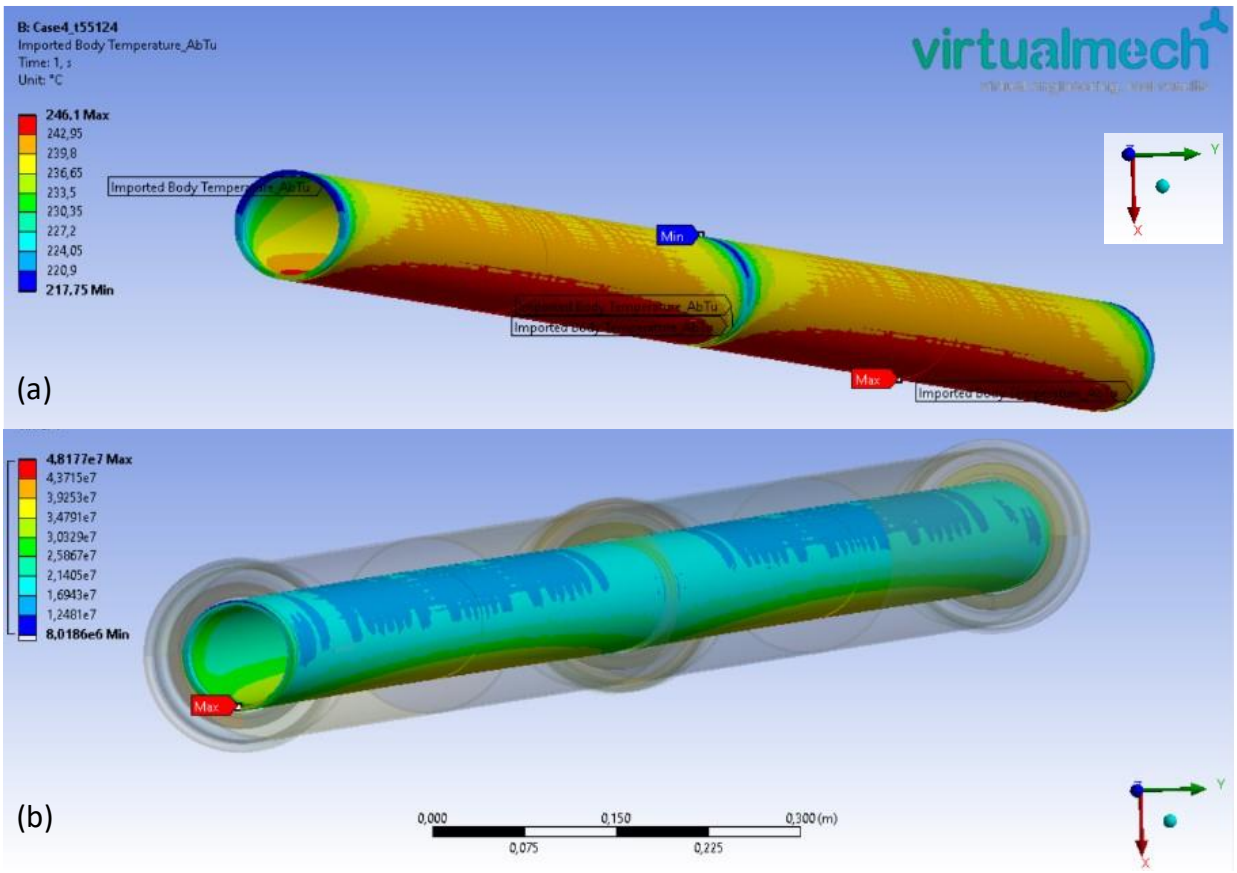

Figure 15: (a) Temperature profile [°C] for a solar heating simulation with 120 s pause off-sun and (b) resulting von Mises Stress profile [Pa] with a maximum of 48.2 MPa occuring at the HCE interconnect.

In summary, the presence of natural convection greatly reduces the circumferential thermal gradients, and thus thermal stresses in the HCEs during solar flux heating; however, the presence of the non-illuminated bellows greatly increases the melt time. With $t_{\text{off}} = 60$ s, close to 12 hours of sun at 1000 DNI are required to complete the melt process with pure solar heating (flex hoses still require electrical heat input). These conditions are extremely challenging for most of the year, if not outright impossible in many locations. It is likely that t_{off} can be reduced further, which could reduce the melt time but also increase stresses; however, additional resources are required to explore the limits of this heating method. For now, the modeling results presented here suggest this method of heating can be safely applied to the solar field; however, the time and weather conditions required to completely melt the salt present challenges for design of a robust freeze protection system. Considering the limitations of Joule heating systems in commercial scale applications [7], the solar flux heating method described above has potential to significantly improve freeze recovery and protection systems in molten salt parabolic trough plants.

6.4 HCE Freeze Recovery Overview

Using both Joule and solar heating in a combined system has potential to provide the robust design needed for commercial applications. Such a system could reduce the capital and operating costs of a Joule heating system, while increasing the flexibility of the solar heating systems for shorter and cloudier

This material is based upon work supported by the U.S. Department of Energy's Office of Energy Efficiency and Renewable Energy (EERE) under the Solar Energy Technology Office Award Number DE-EE0008140.

days. To compare results with different heat inputs the volume and time averaged heat input, $\bar{q}$, is a useful parameter.

$$\bar{q}\ [\mathrm{W\ m^{-1}}] = \frac{1}{t_{\mathrm{cycle}}} \int_0^{t_{\mathrm{cycle}}} \left(q_{\mathrm{imp}} + \frac{R_{\mathrm{o}}}{L} \int_0^{L} \int_0^{2\pi} q_{\mathrm{solar}} \right)$$

A summary of the results completed with the 3D natural convection model is presented in Table 4. In all these cases the maximum von Mises stress of the receiver tube is well below the allowable values in ASME Section II code [15] (129 MPa at 250°C). The solar heating simulation, Case 2, has a similar $\bar{q}$ to the Joule heating simulation, Case 1, yet Case 2 results in a maximum stress that is 8.2 MPa higher and a melt time 6.5 h longer. However, solar heating methods are not limited by current density, so increasing $\bar{q} > 250$ W m^{-1} is not an issue. With $t_{\mathrm{off}} = 60$ s, Case 3 achieves very similar performance to Case 1 while maintaining the HCE integrity. Case 4 shows results for a combined Joule and solar heating simulation, 150 W m^{-1} Joule heating is added to the solar flux profile from Case 3. In this case melting is achieved in 6.75 h with a maximum von Mises stress of 45.7 MPa. If minimizing downtime is the objective, a combined system will provide the fastest and most robust freeze protection for the HCEs in the solar field. If minimizing freeze protection costs is the objective, model results suggest that solar flux heating of the HCEs is feasible, but operational challenges such as weather and cold spots at damaged HCEs will likely increase the solar field downtime after a full freeze event.

Table 4: Summary of results from 3d melting simulations of salt frozen in an HCE, considering density variations. The yield strength of the receiver is 205 MPa, and the maximum allowable stress at 250°C is 129 MPa.

Case	Impedance Heating [W/m]	t_{off} [s]	Melt time [h]	$\bar{q}$ [W m^{-1}]	Max Von Mises [MPa]
1	250	-	11.98	250	39.8
2	0	120	18.52	254	48.2
3	0	60	11.90	386	43.3
4	150	60	6.75	536	45.7

Another aspect to consider for solar or combined heating systems is the formation of a flow path in the HCE loop. As seen in the results in in Sections 6.2 and 6.3, natural convection greatly increases heat transfer during thawing. Once a flow path is formed throughout a loop, forced convection via internal salt flow is also an option. The liquid fraction plotted in Figure 14 indicates that an average liquid fraction of 20% is achieved at around 60% of the melt time, or about 7.2 hours with $t_{\mathrm{off}} = 60$ s. If the heating process is relatively uniform along the length of the flow loop, the salt pumps can be used to increase heat transfer to the frozen media at this point. In a commercial system, a recirculation loop would protect the pumps from potential cold spots which could prevent salt from flowing through the loop, assuming the header piping is thawed prior to the solar field, if necessary.

This material is based upon work supported by the U.S. Department of Energy's Office of Energy Efficiency and Renewable Energy (EERE) under the Solar Energy Technology Office Award Number DE-EE0008140.

7 Outdoor Test System

The encouraging model results for molten salt freeze recovery in receivers described in the previous section do not capture many of the realistic physical complexities present in real-world collector systems; furthermore, the computational resources required to model these complexities are significant. For these reasons, field testing is required to ensure the novel solar heating method can be safely applied to a parabolic trough collector in realistic operating conditions.

The project originally only anticipated indoor testing of interconnections on a test bench during budget period 2. However, because the end of project goal for indoor testing of interconnects was achieved in budget period 1, SD proposed a more aggressive outdoor testing program to DOE for implementation during Budget Period 2. The project was able to leverage a parabolic trough concentrator prototype from a recently completed SunShot project (award no. DE-EE0007121) and an SETO-authorized increase in project budget to install a real-scale molten salt collector test bed to validate the project's model results and test the alternative heating systems developed during this project in a realistic outdoor setting. The molten salt collector test bed was installed at the Solar Dynamics' testing area within the solar Technology Acceleration Center (SolarTAC), located near Watkins, CO.

7.1 Molten Salt Collector Testbed

The molten salt collector testbed consists of a single 8.2m SunBeam™ parabolic trough collector module, 5 receivers (also known as heat collection elements, or HCEs) in length, situated between two 100 gal (379 liters) Department of Transportation ("DOT") rated carbon steel tanks to hold the molten salt. Five Huiyin MS90 HCEs with a total absorber tube length of 20.3 m are connected via Senior Flexonics' RF-Triple® interconnect assemblies to the two DOT rated tanks, which serve as low temperature salt tanks (< 370°C). The Senior Flexonics' RF-Triple® were selected based on the laboratory testing described in Section 5. Each tank is outfitted with two globe valves to control the air pressure in the tank, one vent valve and one supply valve connected to an air compressor. Compressed air is used to "push" salt from one tank, through the flex hoses and HCEs, and into the opposite tank. Although unconventional relative to a commercial system, this simplified method of moving salt eliminated the need for a circulation pump, the return pipe, and all of the associated components that would have otherwise been needed (e.g. extensive heat trace, insulation, expansion loop, etc.).

The trough module can rotate a total of 205°, from 40° below the eastern horizon to 15° above the western horizon as installed, thus providing sun tracking capabilities. The flex hoses are installed in an orientation that allows gravity draining back to the tanks when the collector is positioned slightly above the horizon. Both flex hose assemblies and the string of HCEs are connected to DC power supplies designed to provide 250 W m^{-1} to each component independently. A pre-construction rendering of the test site is shown below in Figure 16.

This material is based upon work supported by the U.S. Department of Energy's Office of Energy Efficiency and Renewable Energy (EERE) under the Solar Energy Technology Office Award Number DE-EE0008140.

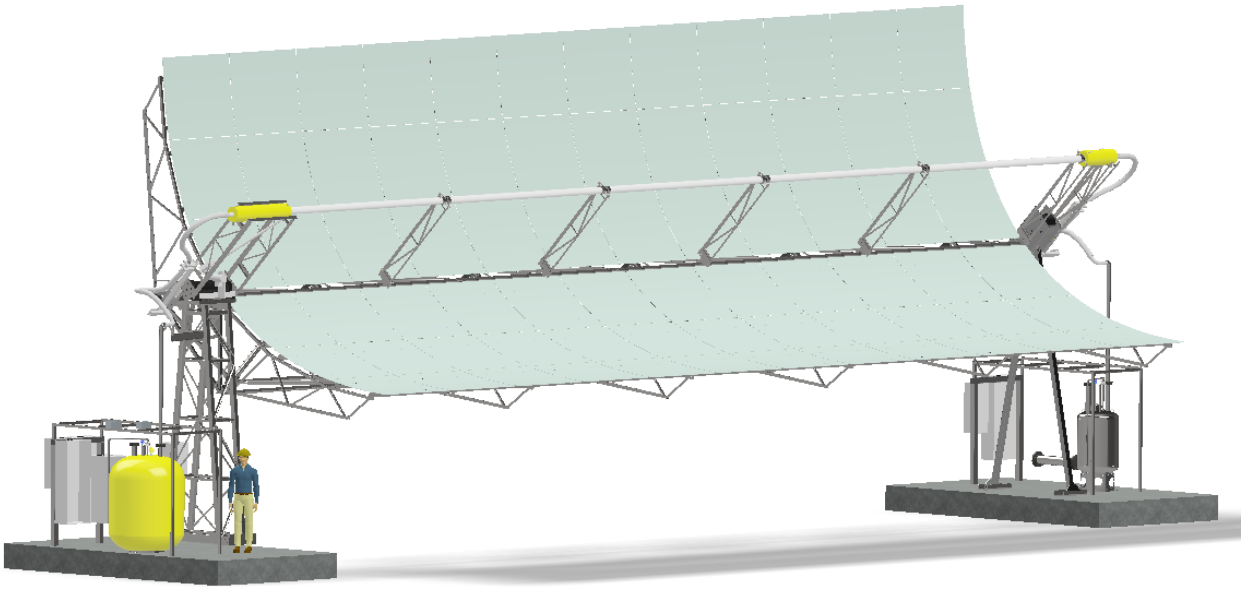

Figure 16. Pre-construction rendering of SMART test site

The test platform was heavily instrumented to support the project test program. An instrumentation diagram is provided below.

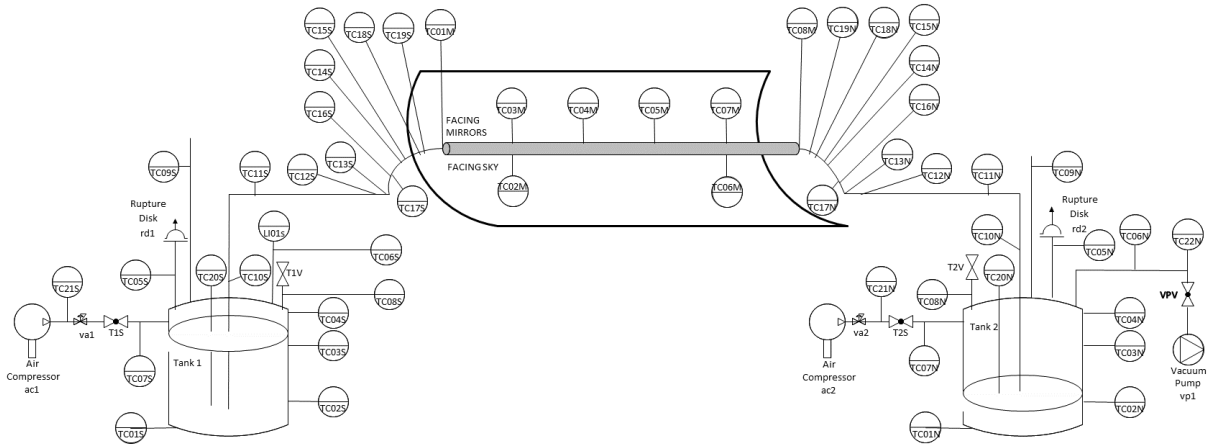

Figure 17. Instrumentation diagram of the test system at SolarTAC.

7.2 Test Site Erection

This section summarizes the test site preparation activities undertaken by this project at SolarTAC. This is captured largely with pictures and brief narratives.

Foundations were poured in mid-December 2019 as seen in Figure 18 below.

This material is based upon work supported by the U.S. Department of Energy's Office of Energy Efficiency and Renewable Energy (EERE) under the Solar Energy Technology Office Award Number DE-EE0008140.

Figure 18. Foundation pouring in mid-December 2019

Trenching was performed for installation of electrical and control cabling within the test site area.

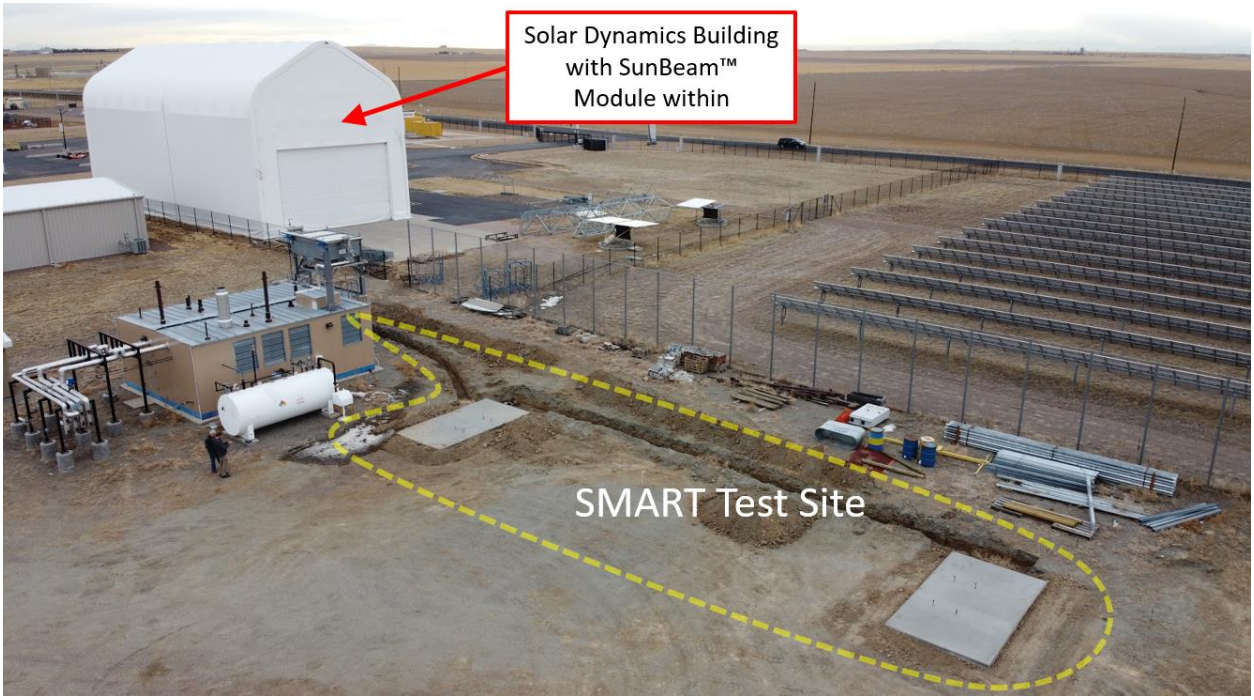

Figure 19. Picture of Test Site in early January 2020

Progress was made on the electrical works during Q1 2020 including all underground conduit for the test site as seen in Figure 20 below.

This material is based upon work supported by the U.S. Department of Energy's Office of Energy Efficiency and Renewable Energy (EERE) under the Solar Energy Technology Office Award Number DE-EE0008140.

Figure 20. Picture of Underground Conduit Installed in Q1 2020

A single SunBeam™ module was made available from the Solar Dynamics "ATLAS" SunShot project [10]. A picture of the collector as of early January 2020 is included below.

Figure 21. SunBeam™ module within Solar Dynamics building at SolarTAC

During Q1 of 2020, the heat collector elements (HCEs) were aligned on welding stands with a jig arrangement utilizing a laser as seen in Figure 22 below.

This material is based upon work supported by the U.S. Department of Energy's Office of Energy Efficiency and Renewable Energy (EERE) under the Solar Energy Technology Office Award Number DE-EE0008140.

Figure 22. HCE welding stands aligned with jig and laser

The string of five (5) HCEs were then welded as shown in Figure 23 below.

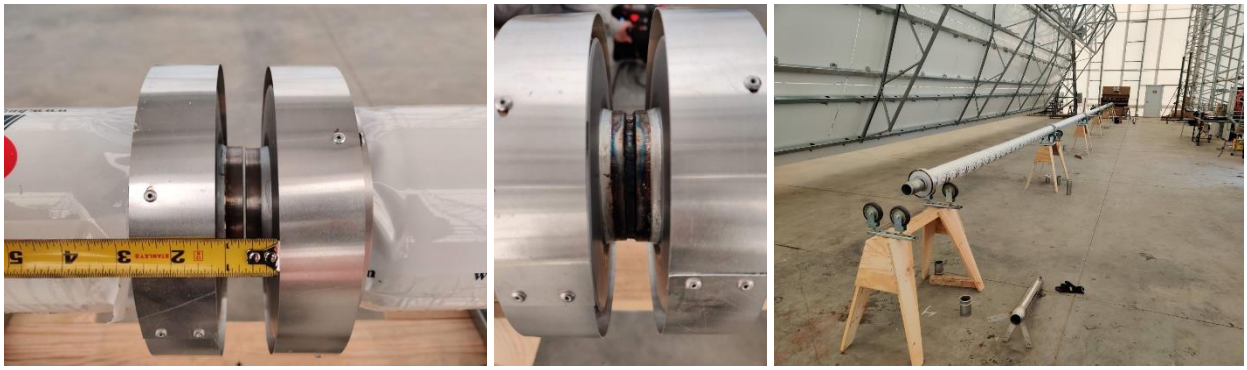

Figure 23. HCE welding process

Finally, the string of HCE's were lifted using a pulley system onto the SunBeam™ module as shown in Figure 24 below. It's worth noting that the HCEs and mirrors were initially installed indoors for the purpose of adjusting and aligning, activities under the ATLAS project. Mirrors and HCEs were then removed to simplify the crane lift to the collector's outdoor location.

This material is based upon work supported by the U.S. Department of Energy's Office of Energy Efficiency and Renewable Energy (EERE) under the Solar Energy Technology Office Award Number DE-EE0008140.

Figure 24. Picture of SunBeam™ module with HCE installed

Wind fence material was added to the western boundary of the test site at seen in Figure 25 below. Predominant winds at this site are from the southwest. The module is protected from southerly winds by pre-existing and unrelated structures at the south of the installation.

Figure 25. Wind Fence Installation on Existing Fence

A crane was used to relocate the trough module on September 16, 2020.

This material is based upon work supported by the U.S. Department of Energy's Office of Energy Efficiency and Renewable Energy (EERE) under the Solar Energy Technology Office Award Number DE-EE0008140.

Figure 26. Crane Operation to Relocate SunBeam™ Module

The welded string of HCEs were moved manually from inside the building to the outdoor test site.

Figure 27. Relocation of HCE

The DOT tanks were installed and MI cable heat tracing was fixed on all surfaces of the tanks prior to insulation.

This material is based upon work supported by the U.S. Department of Energy's Office of Energy Efficiency and Renewable Energy (EERE) under the Solar Energy Technology Office Award Number DE-EE0008140.

Figure 28. Salt Tanks Heat Trace & Insulation

The Senior Flexonics flex hoses were then installed on either end of the module. This operation presented a challenge since the flex hoses are heavy, non-rigid, and difficult to maneuver and bend into their installation orientation. Two differing approaches were used for each of the two flex hoses. In the first approach, two wooden 2x4s were used as splints to keep the hose linear while lifting (Figure 29, left). This approach worked well for maintaining rigidity while lifting, but it was very challenging to bend either end of the flex hose to arrange for welding. In the second approach, the shipping container was partially deconstructed and modified in order to repurpose as a lifting platform (Figure 29, right).

Figure 29. Flex hose rigging and lifting

The second approach was much more effective as it allowed for easier positioning of the flex hose into its final welding orientation, resembling that of a question mark (Figure 30, center).

This material is based upon work supported by the U.S. Department of Energy's Office of Energy Efficiency and Renewable Energy (EERE) under the Solar Energy Technology Office Award Number DE-EE0008140.

Figure 30. Flex hose placement and staging for welding

A few recommendations for commercial scale deliveries of similar flex hose assemblies are: to ship the hoses in the curved orientation in which they are to be installed, make the containers to be easily deconstructed into a platform, and include pre-installed lifting lugs at each corner of the resulting platform.

Figure 31. Flex hose placement and welding

This material is based upon work supported by the U.S. Department of Energy's Office of Energy Efficiency and Renewable Energy (EERE) under the Solar Energy Technology Office Award Number DE-EE0008140.

Figure 32. Inlet and Outlet Valves on South Tank

Figure 33. Joule Heating Power Supplies (left) and Salt Trap (right)

This material is based upon work supported by the U.S. Department of Energy's Office of Energy Efficiency and Renewable Energy (EERE) under the Solar Energy Technology Office Award Number DE-EE0008140.

Figure 34. Picture of Test Site in December 2020

Figure 35. On-sun testing with complete installation

This material is based upon work supported by the U.S. Department of Energy's Office of Energy Efficiency and Renewable Energy (EERE) under the Solar Energy Technology Office Award Number DE-EE0008140.

8 Test Results

The SMART test platform was designed for low-flow molten salt operation up to 350°C, with the intent to validate model results from Section 6 and test the novel freeze protection methods on-sun. The test setup was used to test solar heating with pass-through tracking (see Section 6.3) as a method for pre-heating the HCEs. It is assumed that freeze protection heaters would pre-heat the solar field during commissioning of molten salt trough plants, so these tests are relevant for commercial applications.

All data in the following sections was collected with the test system open to the atmosphere, i.e., compressed air supply valves closed and tank vent valves open. This test setup is usually subject to windy conditions as the site is remote and very exposed. Steady state conditions are very challenging to achieve due to wind and other changing environmental conditions. For these reasons, the steady state conditions described in the following sections could be better described as quasi-steady state: periods of time where the temperature of the component of interest is changing slow enough to be considered constant, in this case the threshold considered is $\frac{dT}{dt} < 1\text{e} - 4$ °C s^{-1} for 30 mins.

8.1 HCE

The string of 5 HCEs was instrumented with 8 Type K thermocouples (“TC” or “TCs”): 6 installed on the outer receiver tube surface at the welded interconnects in between HCEs, and 2 installed in thermowells extending 0.45 m into the illuminated zone on either end of the HCE string. Unfortunately, during the first rotation of the trough structure with instrumentation installed, the south thermowell TC was pulled out of the thermowell and wedged near the metal surface of the spool piece just outside of the illuminated zone, rendering it unusable and preventing installation of a new TC. The thermocouple locations are illustrated in Figure 36. Without the south thermowell temperature reading the data will not capture axial gradients in the HCE due to high solar incidence angles.

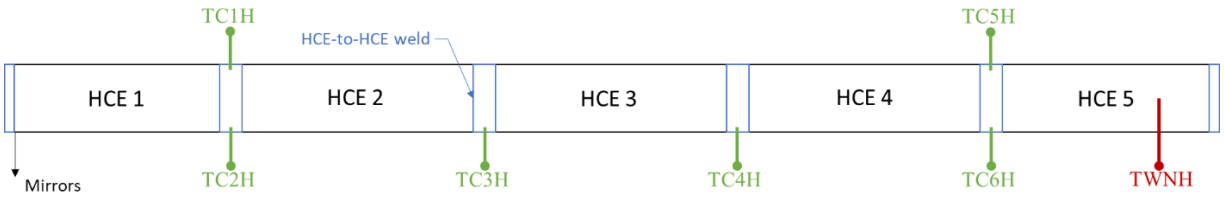

Figure 36: Diagram showing the thermocouple locations as installed on the HCE string at the SolarTAC test site. The red sensor is a thermowell TC.

To evaluate heat losses, the HCE string was allowed to reach steady state conditions with only electrical heating inputs, these results are tabulated in Table 5. The north HCE thermowell temperature (TWNH) is assumed to represent the internal receiver wall temperature in the illuminated section of the HCE, due to radiation exchange with the thermowell tube. This data suggests the bellows and illuminated sections of the HCEs have similar heat losses when $T < 100$°C. Above 100°C the bellows temperature tends to be lower than the thermowell, with a significant $\Delta T = 76.4$°C at the highest steady state temperature recorded; these results indicate increased heat losses from these sections at elevated temperatures.

This material is based upon work supported by the U.S. Department of Energy’s Office of Energy Efficiency and Renewable Energy (EERE) under the Solar Energy Technology Office Award Number DE-EE0008140.

Table 5: Steady state data at various environmental conditions and Joule heating power for the HCE string. The column Avg. TCXH is the average of all measured temperatures at the welded HCE connections.

Time	Avg. TCXH [°C]	TWNH [°C]	Wind speed [m s^{-1}]	Air Temp [°C]	Sky Temp [°C]	Q_{JH} [W m^{-1}]
6/17 1:00 – 1:30	172.8	249.2	4.9	23.2	0.5	135.6
6/19 4:00 – 4:30	148.1	156.7	2.4	15.6	-3.9	73.4
6/21 1:00 – 1:30	121.5	137.4	6.6	11.5	-6.9	74.5
8/11 5:00 – 5:30	114.5	126.4	2.5	13.2	-7.7	46.3
9/21 0:30 – 1:00	75.9	69.0	4.0	17.1	-2.1	23.4
9/24 5:30 – 6:00	93.7	91.3	4.1	17.1	-0.9	37.2

Data for the first track-through heating test performed with the SunBeam™ module and the HCEs filled with ambient air is shown in Figure 37. The HCE string was heated from 27 to 152°C in 70 mins based on TWNH, with a 30 s pause off-sun and rotational speed of 0.32 °/s. After the initial 50 mins of heating, a relatively constant heating rate of 2.9 and 2.2°C per minute was achieved at the HCEs and bellows, respectively, until the mirrors were moved off-sun. During this period the DNI was relatively constant around 500 W m^{-2}. This data suggests the method of heating is a viable option for pre-heating the SunBeam™ trough receivers, and those of other designs with similar rim angle and concentration ratio. Two other tests were performed at similar DNI conditions, with a 30 s and 60 s pause off-sun. The 60 s pause off-sun test heated the HCE string from 26 to 215°C in 139 mins, while the bellows were heated to 168°C; this was the maximum temperature achieved with solar pre-heating. No visible permanent deformations were developed in the HCE string after any of the first three track-through tests; however, further analysis would be required to estimate the potential fatigue damage incurred on the HCEs by pre-heating with this method. Future tests should incorporate a camera fixed to the trough structure, to monitor deflections of the receiver tube during heating and cooling.

This material is based upon work supported by the U.S. Department of Energy's Office of Energy Efficiency and Renewable Energy (EERE) under the Solar Energy Technology Office Award Number DE-EE0008140.

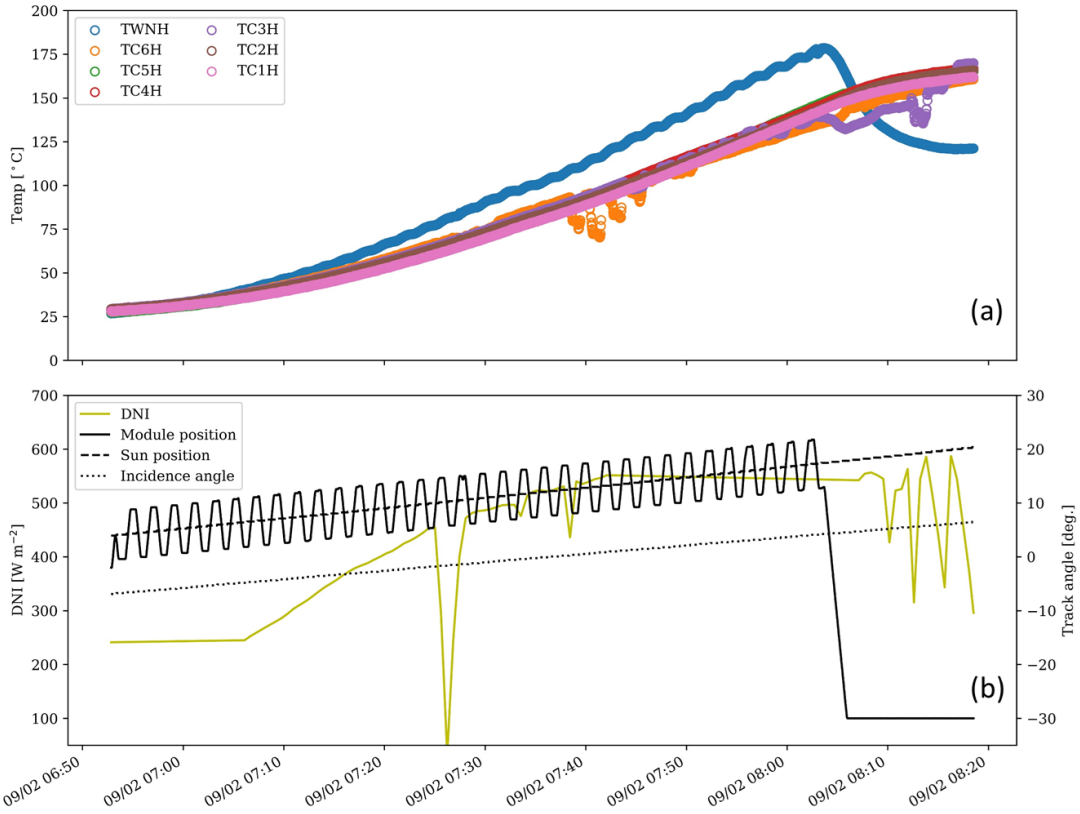

Figure 37: Experimental data for pass-through heating with 30 s pause off-sun: (a) evolution of temperature measurements on HCE string, (b) trough module position and solar conditions during testing. Module position is 0° at horizon position and 90° at zenith orientation. Sun position is the module on-sun position at each time.

8.2 HCE Thermal Model Validation

Experimental validation for the HCE thermal model was performed with air due to challenges maintaining the temperatures required to keep Solar Salt above the liquidus temperature along the entire test loop. The validation was performed using pass-through heating data of an empty HCE. The OpenFOAM model developed for the test site is a thermal model of the solid domains of the HCE. The bellows boundary condition is approximated as an insulated section of receiver tube with an extra source term to account for conduction to the receiver supports. The inner receiver wall is modeled as an insulated surface. As mentioned in Section 1, Huiyin contributed the HCEs installed at the SolarTAC test site; these HCEs are pre-production prototypes and the properties may differ from design specifications. The emissivity, ε, is the most relevant property for the thermal model; ε for the installed receiver was calculated by minimizing the error between the steady state data in Table 5 and results from the HCE heat loss model by Forristall [16].

This material is based upon work supported by the U.S. Department of Energy's Office of Energy Efficiency and Renewable Energy (EERE) under the Solar Energy Technology Office Award Number DE-EE0008140.

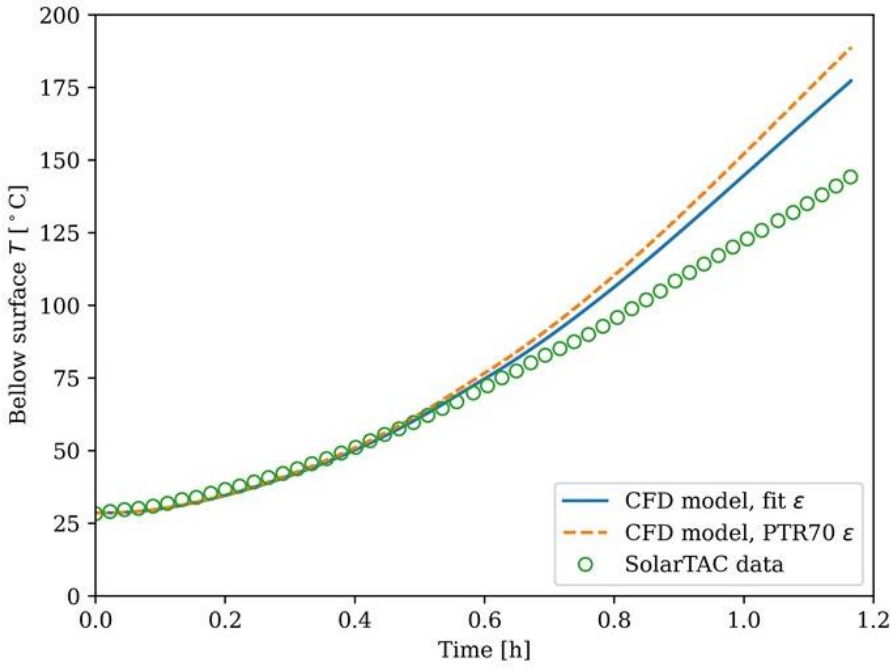

Figure 38*: Comparison of experimental temperature data to simulation results with an insulated inner HCE wall.*

The simulation and experiment are compared using the average of temperature readings TC3H and TC4H from the welded connections closest to the center of the HCE string (see Figure 36). The thermowell temperature is not used for comparison due to the complexity of accounting for the lag time to the sensor with air inside the HCE. The simulation does a good job of capturing the initial heating of the bellows, but as T increases the heat losses in the simulation appear to be lower than those in the outdoor experiment. Model results are compared assuming the HCE receiver tube emissivity, ε, from [17], as well as the fitted value described above. After 70 mins of heating the simulation T is 33°C higher than the measured T for the fitted case, compared to 44°C for the PTR70 case with an ideal function for ε. Despite some improvement with the updated ε function there is still significant divergence from experimental data at higher temperatures, indicating radiative losses are not the main source of error between model and experiment at these temperatures. Based on these results, the thermal boundary condition at the bellows does not do an adequate job of capturing the heat losses from these regions and requires further development. Other sources of error include the presence of natural convection to air within the HCEs, as well as discrepancies between the total flux in Figure 12(a) and the actual flux achieved at the test site.

8.3 Flex hose

The main option considered for heating the RF-Triple® component is Joule heating. Due to the rotation of this component during plant operation, heat tracing is not considered a viable heating method. Each flex hose installed at the outdoor test site was instrumented with 8 Type K thermocouples: 1 underneath the insulation at the inlet and outlet of each flexible hose, 1 in between the 90° elbows outer metal surface, and 1 thermowell in the 90° elbow closest to the module (refer to Figure 3 for flex hose diagram). Significant challenges were encountered with Joule heating the flex hose with stagnant fluid in real world conditions, which ultimately prevented heating of the flex hose above the desired set

This material is based upon work supported by the U.S. Department of Energy's Office of Energy Efficiency and Renewable Energy (EERE) under the Solar Energy Technology Office Award Number DE-EE0008140.

temperature. The main issues identified were increased heat losses from the hard pipe sections connecting the flexible hoses, and uneven heat input from the DC power supplies due different resistance values in the hard pipe versus flexible hoses.

The resistance of each component is a critical parameter for designing the Joule heating system. The resistance and heat losses of the flex hose were measured in a lab setting at the University of Wisconsin at elevated temperatures; this data provided the basis for design of the Joule heating system installed in the outdoor test. Discrepancies between the two test setups resulted in a relative difference of about 50% between the resistance per unit length values measured at the SolarTAC test site and the UW lab, resulting in the power supplies being sized inappropriately. A portion of the difference in predicted and observed resistances for the outdoor test setup is attributed to the different lab-scale test not having the receiver thermal expansion hose installed (see Figure 3 and Figure 7). The different composition of the flexible hose and solid pipe portions of the flex hose, quantified in Table 6, results in a 10.8% difference the $\Omega\ m^{-1}$ value of the two tests. The remaining discrepancy is attributed to electrical connections and measurement error, which can be significant factors due to the relatively small values of resistance in question (around 10 mΩ).

Table 6: Calculated resistances for the different sections of the RF-Triple® assembly at 145°C.

	Total (measured, SolarTAC)	**SS316L (theoretical)**	**Flexible Hose (calculated)**
$r\ [\mathrm{m\Omega\ m^{-1}}]$	2.056	0.745	2.402
$L\ [\mathrm{m}]$	5.245	1.095	4.150
$R\ [\mathrm{m\Omega}]$	10.79	0.815	9.970

The resistance values in Table 6 result in non-uniform heat inputs along the length of the flex hose when the fluid inside the component is stagnant. In addition, the 90° elbows and support arm appear to have higher heat losses in an outdoor setting compared to the flexible hose sections. The variation in heat inputs and losses is illustrated in Figure 39(a). This conclusion is supported by the steady state temperature profiles plotted in Figure 39(b), where the combination of increased heat losses and lower heat input results in a clear cold spot at the 90° elbows. Although there is no temperature sensor installed on the support arm, the increased heat losses of this component clearly effect the temperature readings TC5F and TC6F in the 2021-06-19 dataset. To alleviate this issue additional insulation was installed on the 90° elbows and support arm of the installed flex hose assembled (see Figure 3). The added insulation reduced the steady state temperature difference across the RF-Triple® assembly from 64.1 to 38.6°C, as seen in Figure 39(b).

During normal plant operation, advective heat transfer due to the HTF flow would reduce thermal gradients in the RF-Triple® significantly; however, during a freeze recovery event where initial heating is expected to occur without flow, the observed thermal gradients could be problematic. In this case, the discrepancy in resistance values and non-uniform heat input/outputs resulted in the Joule heating system incapable of heating the RF-Triple® to the desired operating temperatures. Due to the mechanism of heating in this system, the solid lengths of pipe with lower resistance dissipate less heat

This material is based upon work supported by the U.S. Department of Energy's Office of Energy Efficiency and Renewable Energy (EERE) under the Solar Energy Technology Office Award Number DE-EE0008140.

compared to the higher resistance flexible hose sections. To achieve the desired level of heating at the SolarTAC test site, a power supply with the same output power but a higher current rating should be used, i.e., 2.4 kW at 400 A. However, a different power supply would not change the thermal gradients present in the system. Potential solutions to further reduce the axial gradients include: 1) more insulating materials such as a wind/radiation shield, 3) increasing the resistance of solid pipe sections by lowering the wall thickness. Changing from schedule 40s to schedule 10s or schedule 5s piping would increase the resistance of the SS316L sections by 64% or 134%, respectively (from Table 6: flex hose Ω m^{-1} is 222% greater than SS316L sections). While reducing the wall thickness would be the best long-term solution for Joule heating, further analysis is required to ensure a lower wall thickness is acceptable structurally at operating temperature and pressure.

This material is based upon work supported by the U.S. Department of Energy's Office of Energy Efficiency and Renewable Energy (EERE) under the Solar Energy Technology Office Award Number DE-EE0008140.

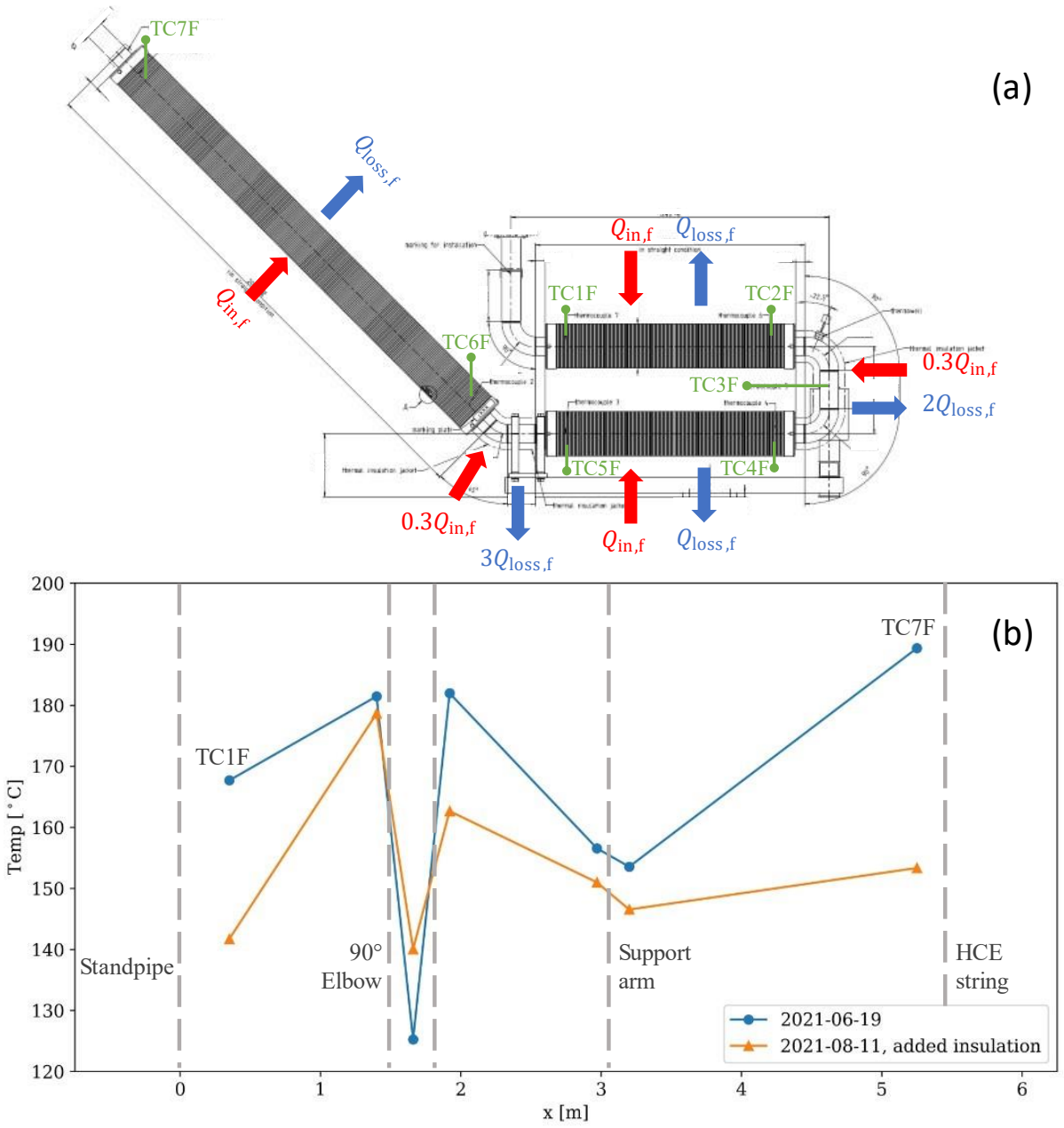

Figure 39: (a) Temperature sensor locations and estimated non-uniform heat losses and Joule heat inputs on the RF-Triple® component, Q values in W m^{-1}. (b) Steady state temperature profile along the length of the flex hose before and after adding insulation at similar ambient conditions (13 – 16°C, 2 – 3 m s^{-1} wind speed).

8.4 Limitation of Modeling and Testing Under the Project

The end goal of the outdoor testing was to test the freeze and thaw of salt in the receivers and flex hoses. This testing would serve to demonstrate the feasibility of freeze recovery utilizing combinations of Joule heating and the solar "track through" method. Unfortunately, this testing was not able to be conducted for a number of reasons. The Joule heating system had some design discrepancies. The sizing of the power supplies for the Joule heating system were based on the electrical resistances of the HCE string as well as the flex hoses. The electrical resistance of the HCE string was calculated based on

This material is based upon work supported by the U.S. Department of Energy's Office of Energy Efficiency and Renewable Energy (EERE) under the Solar Energy Technology Office Award Number DE-EE0008140.

material electrical properties in combination with the geometry. The electrical resistance of the flex hose was based on measurements from a prior test article that was smaller than the articles at SolarTAC test site. Unfortunately, both resistances of the HCE string and full size flex hoses were nearly 50% different than the calculated values, resulting in purchased power supplies that were unable to reach their maximum power due the limitations of voltage or current.

Additional barriers to project testing included unforeseen circumstances including COVID-19, procurement delays, and construction delays, resulting in the project running out of time and budget to be able to conduct such tests. As a result, some remaining tasks and questions remain.

Furthermore, the freeze recovery process is especially challenging to model, so testing will be critical to prove the functionality of the novel freeze recovery system. Several questions remain regarding this process and the potential solutions, which could benefit from further scientific research, testing, and design efforts:

- How does non-uniform heat input effect the melting cycle? (e.g. shading from high incidence angle solar flux)
- Characterization of void spaces which may form in HCEs and piping during the freeze cycle. What is the distribution of void space around a loop?
- What are the physical properties of Solar Salt in the “mushy” zone (through the solid-liquid phase transition)?
- How much pressure might be required to dislodge a plug of solid salt that may be constraining an expanding liquid during the melting process?
- Although impedance / Joule heating systems have been widely used in many applications and are technically very simple, CSP applications are widely reported to experience challenges in practice due to unintended current paths or electrical ‘leaks’ due to the wide variety of metal conductors near the HCEs, e.g. insulation cladding, receivers supports, pylons, the collector structure, etc. Significant design effort is needed to eliminate these potential electrical paths for high quantity commercial deployments.

This material is based upon work supported by the U.S. Department of Energy’s Office of Energy Efficiency and Renewable Energy (EERE) under the Solar Energy Technology Office Award Number DE-EE0008140.

9 Mobile Joule Heating System

This section outlines the design of a mobile Joule heating system for a parabolic trough CSP plant using molten salt as the heat transfer fluid and energy storage medium. The Joule heating system operates on "Joule heating," allowing electricity to flow through the pipe network, generating heat from the energy dissipated in the resistance of each component. A mobile system, which can be temporarily connected to a single collector loop, offers cost savings over a permanently installed plant-wide system. The Joule heating system is intended for three primary functions:

- Preheat a collector loop before initial filling with molten salt (in addition to subsequent filling operations following any maintenance tasks that require draining).
- Freeze protection for a collector loop which has experienced a loss of flow.
- Thawing a collector loop which has frozen after experiencing a loss of flow over an extended period.

Although the third function is expected to have the lowest frequency throughout the life of a plant, it is largely the focus of the design since it is the most demanding, most challenging, and most sensitive use case. Previous studies considering freeze recovery of parabolic trough plants looked at permanently installed systems with various arrangements for wiring and transformer configurations. While this seems like a feasible technical solution these systems have high costs (estimated 80 $/m2) [4], and the power input to the solar field could be limited by the electrical grid capacity resulting in significant downtime [7]. Considering these limitations, a mobile freeze recovery system has potential to offer similar freeze protection capabilities at a fraction of the cost, in exchange for added operational complexity in the freeze recovery process. These potential benefits motivated the design of a mobile Joule heating system for freeze recovery of parabolic troughs.

9.1 Joule Heating System Design

As the design of the Joule heating system is fundamentally an electrical problem, each collector loop is considered as a series of electrical resistance elements. The entire circuit is electrically isolated from the structural components of the solar collectors, but the inlet and outlet pipe connections present potential electrical paths to ground. The Joule heating system may connect at any point between the resistance elements described in the table below.

Table 7. Electrical resistances of each component of the Joule heating system

Component	**Resistance per unit length** [Ω/m]	**Component Length** [m]	**Electrical Resistance** [Ω]	Symbol
HCE string for one module	0.0007790	20.64	0.01608	R_{HCE}
Triple Flex hose	0.002425	3.702	0.008976	$R_{tri\text{-}hose}$
Expansion Flex hose	0.002425	1.750	0.004243	$R_{x\text{-}hose}$
Crossover pipe	0.0004111	20.75	0.008530	$R_{crossover}$

This material is based upon work supported by the U.S. Department of Energy's Office of Energy Efficiency and Renewable Energy (EERE) under the Solar Energy Technology Office Award Number DE-EE0008140.

All resistance values have a level of uncertainty due to variations in temperature, manufacturing and construction variables, potential design modifications, etc. A collector loop consisting of 8 collectors (6 full collectors + 2 half collectors), totaling 70 modules, is depicted dimensionally in Figure 40.

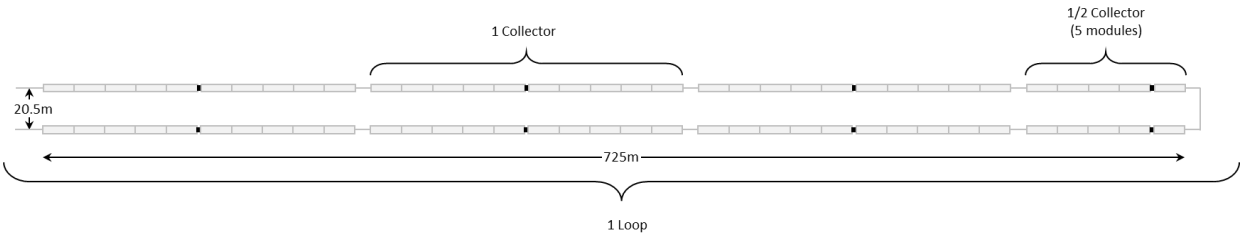

Figure 40. Overall layout and dimensions of SunBeam™ collector loop of 70 modules

The same collector loop is represented electrically in the diagram of Figure 41, corresponding with the electrical resistances identified in Table 7.

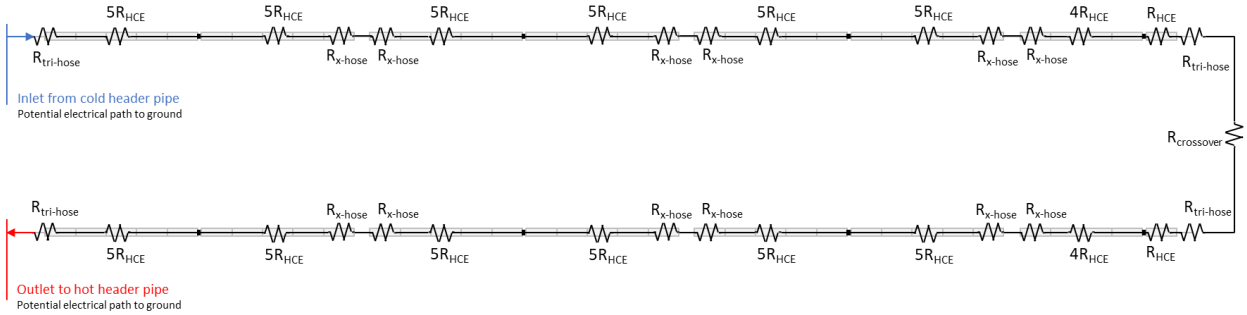

Figure 41. Electrical representation of 70-module SunBeam™ collector loop

Previously proposed Joule heating systems for parabolic trough collectors have focused on solutions for each row of collectors (i.e. half collector loop) [8] or each individual collector [7], applying a positive voltage at one end of the row with a negative terminal at the other end. This presents multiple challenges:

1. A wire of the circuit must span the entire length of the collector row, adding significant cost considering that these wires are very high current and thus very heavy gage.
2. Code requirements limit the allowable voltage that can be applied to piping for exposed DC circuits. The most relevant code reference for this application seems to be NEC article 110.27 which limits the voltage to less than 50V. With such limits and the competing need to achieve higher currents for greater heat generation, the length of the circuits must be much shorter than the length of a collector row.
3. A collector row is inherently non-symmetric since one end is connected to a header pipe (likely electrical ground) while the other end is connected to a crossover pipe.

This material is based upon work supported by the U.S. Department of Energy's Office of Energy Efficiency and Renewable Energy (EERE) under the Solar Energy Technology Office Award Number DE-EE0008140.

An alternative approach is to apply a design solution to an entire collector loop since it is effectively symmetric about a centerline between the two collector rows. DC power supplies can split their current between identical portions of each collector row. Furthermore, each adjacent power supply can be arranged to be opposed to one another in order to limit the maximum voltage anywhere in the circuit. We call this the "Staggered Polarity Concept" and it is depicted in Figure 42 below.

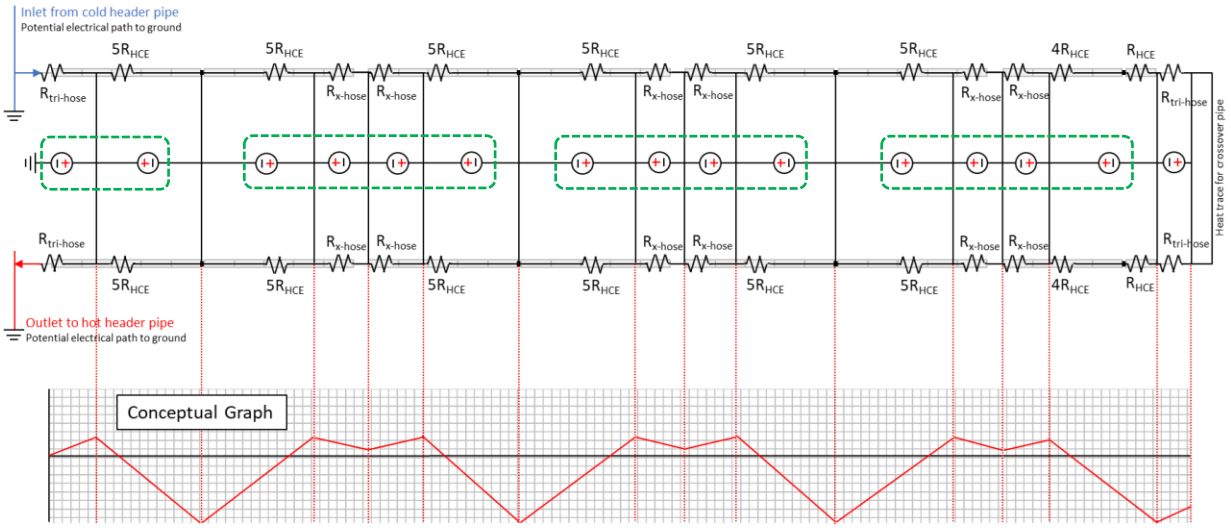

Figure 42. "Staggered Polarity" joule heating concept for a 70-module SunBeam™ collector loop (top) with corresponding depiction of voltage of each row (bottom)

Although the 15 power supplies may appear to be scattered over the 170m length of this collector loop, they can be physically segregated into containers nearest the end of each collector as indicated by the green boxes. Furthermore, the one wire spanning the length of the collector loop covers the needs of two collector rows instead of just one.

As described earlier, this system is expected to be used in rare occasions and it is also very expensive, so a mobile system has been conceptualized that can be temporarily connected to any loop in the power plant. The four green boxes in Figure 42 represent mobile trailer units containing the power supplies with a physical representation of the mobile system shown in Figure *43*.

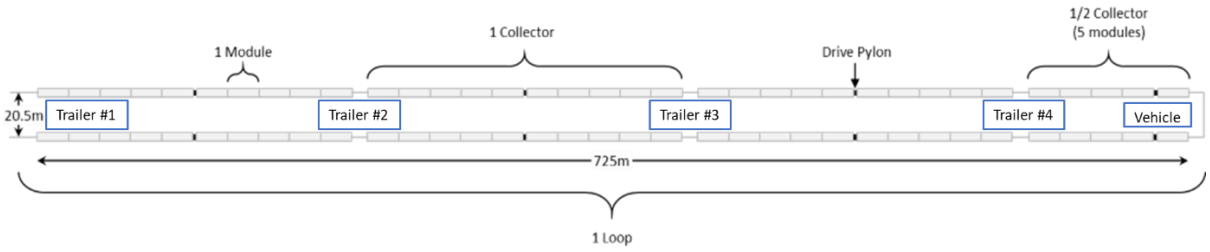

Figure 43. Physical layout of collector loop and approximate trailer locations.

Advisian (Worley Group) was contracted to develop a Design Basis document for the mobile joule heating system, the details of which have informed the design in Section 9.2.

This material is based upon work supported by the U.S. Department of Energy's Office of Energy Efficiency and Renewable Energy (EERE) under the Solar Energy Technology Office Award Number DE-EE0008140.

9.2 Direct Current (DC) Joule Heating Electrical Design

The required electrical heating Watts per meter across the HCE (Heat Collector Element) and interconnecting flexible hose is controlled by the electrical current magnitude through these elements, which is controlled by adjusting the voltage input. Permanent electrical terminals on the piping allow the connection of temporary electrical cables. The cold header pipe and hot header pipe are grounded, while the HCE collector pipe, interconnecting hoses and cross over piping are electrically insulated from ground. The power supplies are installed on four trailers and a vehicle to allow the proper spacing of the power supplies. The power supplies are interconnected in series with their outputs staggered polarity. The maximum power supply operating voltage will be limited to a maximum of 60 VDC across the individual power supply output terminals. Only the output terminal of the power supply immediately adjacent to the header piping is grounded. With the staggered polarities and voltage drop of the interconnecting portable cables, the maximum voltage from any section of piping to ground will be less than 50 VDC when the Joule heating current is operating at design conditions. Each trailer and the vehicle has a ground bus for grounding the equipment frames and AC generator neutral bond, and ground receptacle provisions for a grounding cable connection to a local permanent grounding well that is bonded to the plant main ground grid. Trailer 1 has provisions to bond the power supply output terminal at the header pipe connection to ground.

9.2.1 Codes and Standards

NFPA 70

All electrical components shall be UL listed or contained in UL listed assemblies.

Components and devices not rating for outdoor installation shall be installed inside a weather protected enclosure

9.2.2 Reference Documents

308010-00182-02-EL-DSL-0003; Impedance Heating Electrical One Line (DC)

308010-00182-02-EL-DSL-0003; Impedance Heating Electrical One Line (AC)

9.2.3 Engine Generator

Self-contained with integral fuel, cooling and start system

Integral vibration isolation

Generator 105°C prime rating

277/480V, 3 phase, 60 Hz, synchronous generator with brushless rotating field with an excitation system including a volts/Hz solid state voltage regulator with supplied by a shaft driven permanent magnet generator (PMG). Operation is isochronous with +/- 0.5 percent voltage regulation.

Integral generator output thermal magnetic circuit breaker.

A UL 142 fuel tank with a minimum of eight hours of fuel at rated kW

Communications capabilities for remote indication of status and alarms.

This material is based upon work supported by the U.S. Department of Energy's Office of Energy Efficiency and Renewable Energy (EERE) under the Solar Energy Technology Office Award Number DE-EE0008140.

9.2.4 Power Supply Enclosure

The 480VAC distribution system connects the electrical output from the generator circuit breaker to the thermal magnetic branch circuit breakers supplying the 480VAC inputs to the power supplies.

Direct Current (DC) power supplies;

- Seven (7) EMHP 60-1500: TDK Lambda EMI model number EMHP-60-1500-X-4-4X214; 60VDC, 1500ADC, 414-506VAC input voltage, 57-63Hz.
- Eight (8) ESS 7.5-1000: TDK Lambda EMI model number GEN 7.5-1000-XXX-3P480; 7.5VDC, 1000ADC, three phase 480VAC input voltage, 47-63Hz.
- Power supplies shall have remote communication capabilities with a minimum of the following functionalities.
    - Remote measurement of real time terminal voltage and current.
    - Remote setting of direct current output.
    - Remote On and Off
- Power supplies shall have adjustable maximum voltage and output current limit settings.

The direct current (DC) distribution system interconnects the outputs of the DC power supplies with the output power receptacles.

9.2.5 Receptacle Panel

NEMA 3R/4 receptacles are mounted on receptacle panels as the fixed side of single pole locking type separable connections. Positive polarity receptacles are red and negative polarity receptacles black. The rear threaded connector is connected to the DC power supply outputs by way of the DC distribution system. The contacts of the external connection are recessed and provided with protective caps on lanyards.

Each trailer will have a minimum of one green ground receptacle. The rear threaded connector is connected to the trailer ground bus, at which the generator neutral is connected and the bonding point for equipment ground connections.

9.2.6 Portable Cable and Cable Reels

The portable cables provide the connections between the trailer DC power output receptacles and the HCE electrical termination points. The trailer plug end of the cable will be a 500kcmil Class 1 stranded copper conductor with 600V 90°C PVC/Nylon insulation. Three meters of #2/0 AWG class H stranding nickel coated copper with 500°C insulation is spliced to the HCE termination end of the cable. The inline compression splice shall be watertight. The cable lug shall be high temperature nickel and mechanically compatible with the HCE electrical permanent terminal. The plug on the cable end shall be listed for use with the associated receptacles on the trailers. The plug electrical contacts shall be recessed and provide strain relief for the connected cable. The plug assembly shall be NEMA4 with a lanyard attached NEMA 3R protective cap. Plug bodies shall be red for positive conductors and black for negative conductors.

The trailer portable grounding cables plug bodies shall green. The ground grid end shall have a C-Type Grounding Clamp with smooth jaws and a minimum connection range of 250kcmil to #2/0 AWG.

A trailer mounted cable reel shall be provided for each set of cables to a HCE temporary connections. Reels shall be conservatively sized with different number of wraps in each layer.

This material is based upon work supported by the U.S. Department of Energy's Office of Energy Efficiency and Renewable Energy (EERE) under the Solar Energy Technology Office Award Number DE-EE0008140.

9.3 Mobile Joule Heating System Cost Estimate

An engineering cost estimate for one mobile system consisting of 1 vehicle with 4 trailers, 15 power supplies, 5 engine generators, and all other ancillary equipment is $1.43 MUSD. A Peaker Power plant consisting of 76 collector loops would be advised to own four of these systems, for a total capital cost of $5.72 MUSD. While this might seem expensive, this amounts to approximately $6.60/$m^2$, a small fraction of the baseline $80/$m^2$ of a permanently installed Joule heating system [4].

This material is based upon work supported by the U.S. Department of Energy's Office of Energy Efficiency and Renewable Energy (EERE) under the Solar Energy Technology Office Award Number DE-EE0008140.

10 SAM Molten Salt Trough Performance Model

One of the goals of this project was to improve the bankability of the technology by improving the tools available for modeling parabolic trough plants that use molten salt as the HTF. It is important that validated and publicly available tools are available to evaluate the designs and performance projections of plants. NREL's Solar Advisor Model (SAM) modeling platform is often used by independent engineers supporting investors and lenders to evaluate commercial CSP projects. We reviewed SAM and determined that it allows users to simulate molten salt as the solar field HTF within the Physical Trough Model (PTM). However, there were several shortcomings that prevented it from realistically modeling the most likely configurations for molten salt trough plants. Solar Dynamics contracted NREL to support several upgrades to SAM.

The main shortcomings identified for modeling molten salt trough plants were:

- The collector interconnect definitions were hard coded in SAM's internal piping model to use ball joint assemblies. Unfortunately, ball joints assemblies have not been demonstrated to be feasible for use with molten salt. Other interconnect solutions have been proposed for use with molten-salt. These have significantly different hydraulic and heat loss characteristics than ball joint assemblies. NREL adapted SAM to allow the types of collector interconnection configurations under consideration to be modeled directly in SAM.
- SAM includes a solar field piping model that automatically selects and sizes the piping in a parabolic trough power plant. The piping model in SAM was internal to the model and did not allow the user to influence the piping design or even see the resulting design selected. NREL adapted SAM to allow the user to have more control over the solar field piping design, and output the final piping design so that more accurate costing of the piping, heat tracing, and insulation was possible.
- For molten salt plants, the solar field must be kept warm at night to prevent the salt from freezing. The default overnight operation in SAM was to recirculate the salt and run a heater to maintain the salt temperature above the freeze point. However, the likely commercial design would be to circulate salt from the cold storage tank through the solar field and back to the cold salt tank. This has several advantages, but most importantly it eliminates most of the need for electric or fired heaters during the night.
- In SAM, the default system configuration assumes that HTF exiting the solar field can either flow to the thermal storage or to the power block. In molten-salt trough plants, the solar field will be decoupled from the power block in the same manner as the receiver in a molten salt power tower plant. The solar field and power block are decoupled such that solar collection is independent from power generation.

Solar Dynamics collaborated with NREL to address these shortcomings from the PTM as detailed in the following sections. The public SAM version v2018.11.11 includes the following model updates, accessed through SAM's LK scripting language. NREL published a video and presentation on the updates titled "Updates to the Physical Trough Model in SAM 2018.11.11, Nov 2018" found under the CSP Videos section on the SAM website (https://sam.nrel.gov/).

The latest version of SAM v2020.11.29 uses the plant controller from the MS tower model. This improves mass and energy conservation and plant control, but unfortunately NREL was unable to keep

This material is based upon work supported by the U.S. Department of Energy's Office of Energy Efficiency and Renewable Energy (EERE) under the Solar Energy Technology Office Award Number DE-EE0008140.

the option for independent solar collection and power generation loops. Thus, this option is currently not available in the latest SAM version; NREL plans on adding this feature back in a future release.

10.1 Interconnect Definition

A new robust interconnection procedure is now in place. The user creates an interconnect component library by defining geometry and ΔP loss terms for individual components within a csv file. The format for this file is shown in Table 8. The components within this component library file are then drawn from when defining an interconnect assembly.

Table 8. Example interconnect component definition

Name	Description	Minor Loss Coeff.	Flow Diameter	Length	Type
Units	-	-	m	m	-
e1	Expansion 1	0.15	0.085	NA	fitting
c1	Contraction 1	0.05	0.085	NA	fitting
l1	Elbow 1, long	0.6	0.085	NA	fitting
p1	Pipe 1	NA	0.0635	0.5	pipe
f1	Flex hose 1	0	0.0635	1	flex hose

Interconnect assembly definitions are stored in a separate csv file where the order in which assemblies are listed is the order in which they are assigned to the interconnect locations within the loop. Each interconnection may use a unique interconnection assembly. Figure 44 presents an example expansion only interconnect with flex hoses and the corresponding model definition.

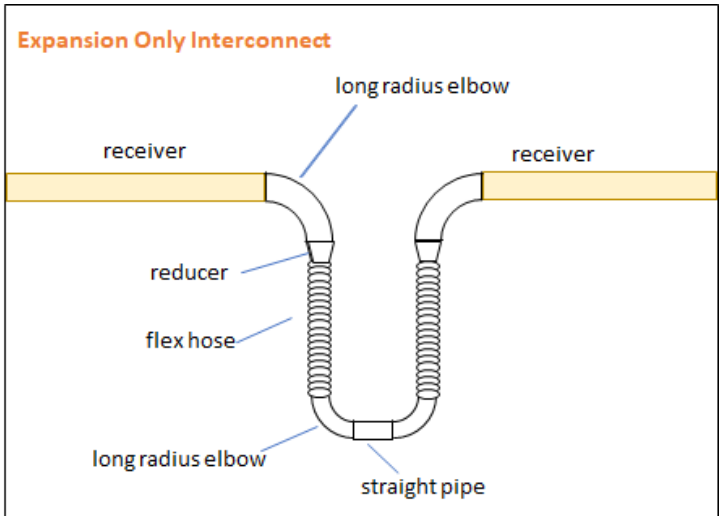

Name	Description	Components
Units	-	-
I#1	Interconnect #1	l1-c1-f1-l1-p1-l1-f1-e1-l1

Figure 44. Interconnect assembly schematic and model definition example

10.2 Solar Field Piping Model Reporting

The PTM now reports the following metrics for each pipe segment in the solar field piping:

This material is based upon work supported by the U.S. Department of Energy's Office of Energy Efficiency and Renewable Energy (EERE) under the Solar Energy Technology Office Award Number DE-EE0008140.

- Diameter
- Length
- Mass flowrate
- Flag if pipe segment includes expansion loop
- Design point velocity
- Design point temperature
- Design point gauge pressure

This information is used within an external detailed cost model for the solar field piping. This step is critical for accurately assessing the cost for molten salt trough plants due to their cost increase over oil-based troughs due to the addition of freeze protection on all solar field piping and the use of stainless steel for all piping between the loop outlet and the hot tank.

10.3 Decoupled Collection and Generation Flow Loops

The last main update is a new flow configuration where collection and generation flow streams are decoupled. This follows the same arrangement of a molten salt power tower. The new arrangement is shown in Figure 45. The new flow configuration also circulates molten salt through the cold tank during nighttime recirculation in the solar field. The cold tank acts as a thermal reservoir that minimizes the need for electrical freeze protection energy overnight.

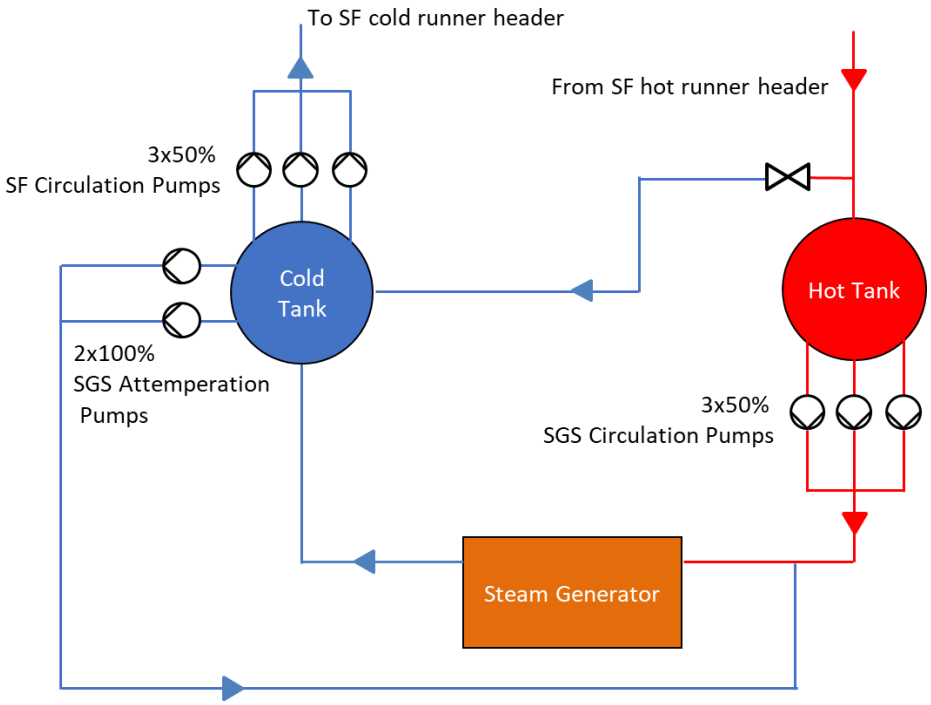

Figure 45. Decoupled collection and generation flow loops

10.4 Integrated System Model

An integrated system model was created that combines Solar Dynamics' developed sizing and cost models with NREL's Physical Trough Model and Financial Models. NREL's models are integrated through the SAM SDK. Figure 46 presents the discrete modeling steps that represent the integrated system

This material is based upon work supported by the U.S. Department of Energy's Office of Energy Efficiency and Renewable Energy (EERE) under the Solar Energy Technology Office Award Number DE-EE0008140.

model. This model enables accurate description of the performance and cost of molten salt trough plants.

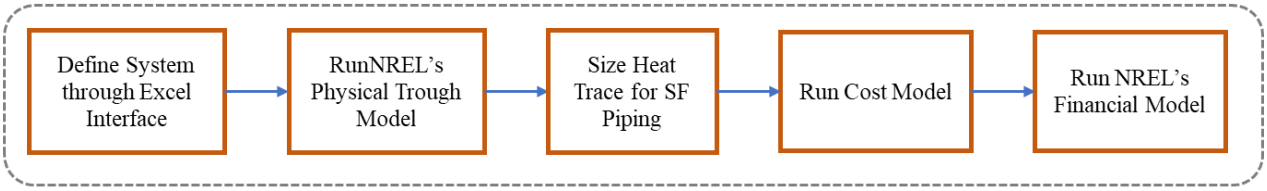

Figure 46. Excel based Integrated System Model

This material is based upon work supported by the U.S. Department of Energy's Office of Energy Efficiency and Renewable Energy (EERE) under the Solar Energy Technology Office Award Number DE-EE0008140.

11 MS Trough Plant Design Optimization

11.1 Commercial MS Trough Plant Design

A commercial parabolic trough plant using molten-salt as the HTF will have a number of important differences from conventional oil based HTF parabolic trough plants. In our design, we assume the following:

1. The process design is changed such that salt will be pumped from the cold storage tank through the solar field and back to the hot tank. When the power plant is operated, salt will be taken from the hot tank and sent to a salt to steam generator to produce steam to operate the power plant. This configuration is similar to a molten salt power tower plant.

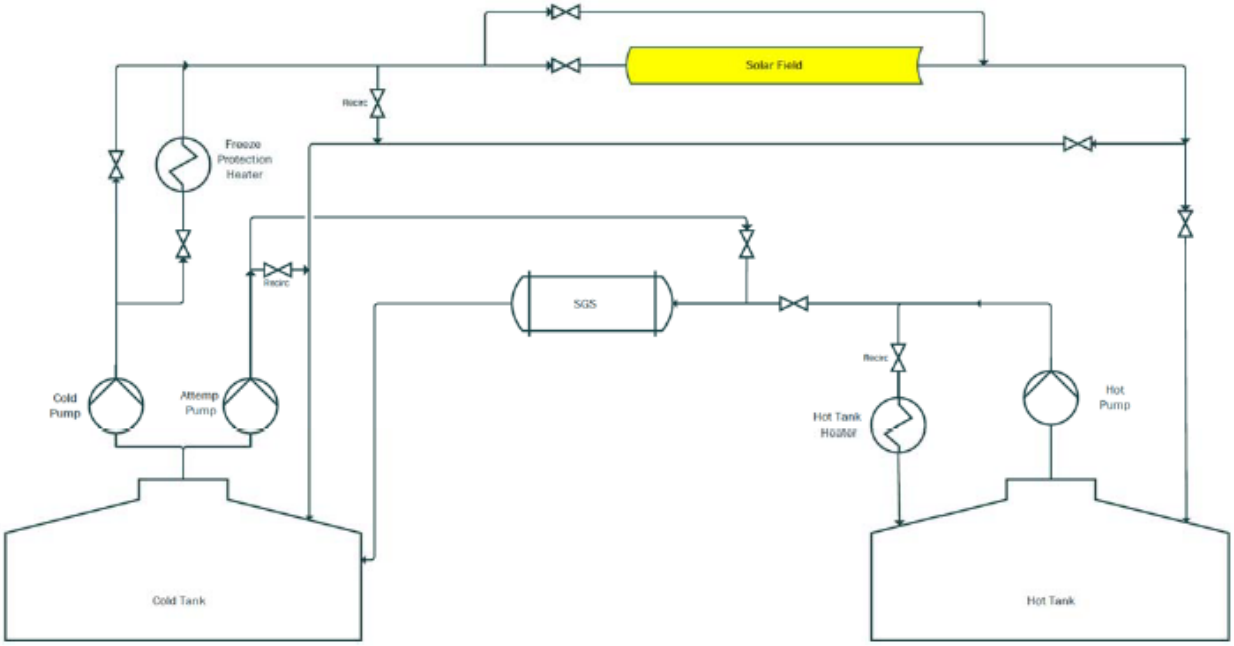

Figure 47. Molten Slat Trough Plant Process Design

2. In general we assume the plant needs to be designed to recover from salt freeze incidents. All of the HTF piping must be heat traced to prevent freezing and/or recover from salt freeze incidents. The collector loop piping and receiver tubes (HCEs) need to be able to allow maintenance on collector loops and recover from salt freezing. We assume loop piping up to the interconnects is heat traced, and the interconnect piping and receivers are heated by impedance heating.
3. During the night, salt from the cold salt tank will be circulated through the solar field and back to the cold salt tank to prevent salt from freezing in the solar field or HTF header piping.
4. A back up salt heater needs to be included in the plant (either electrical or fuel fired), to provide back up heat during extended outages for weather or maintenance.

This material is based upon work supported by the U.S. Department of Energy's Office of Energy Efficiency and Renewable Energy (EERE) under the Solar Energy Technology Office Award Number DE-EE0008140.

11.2 Design Basis Document

Because a molten salt trough plant is a new and unproven concept, we felt it was important to share as much information about the unique aspects of the plant design as possible.

Advisian (Worley Group) prepared a design basis document and associated budgetary cost estimates for the SMART MS Trough Project. There are two plant configurations covered by the Conceptual Design Basis; a baseload plant and a peaker plant.

The Conceptual Design Basis is a 64-page document defining the general design criteria, process/mechanical design criteria, electrical design criteria, I&C design criteria, and Civil/Structural Design Criteria [18].

11.3 Molten Salt Parabolic Trough Collector

The following are common design adaptations employed for molten salt parabolic trough collectors:

- A large aperture width and long collector array, to minimize the number of receivers, collector arrays, loops, and associated specialized process system components (freeze protection and recovery system circuits, flexible piping interconnects, salt-compatible valves and instruments, etc)
- High optical accuracy and rigidity, to support high concentration ratio and long array length
- Molten-salt and/or high-temperature-adapted collector components
    - Salt-optimized HCEs incorporating salt-compatible steels, selective coatings optimized for higher operating temperature, and bellows optimized for greater thermal expansion
    - Collector HCE support arms engineered to accommodate greater receiver string movement under thermal expansion, greater difference between loop inlet and outlet temperatures during operation, and greater weight of the salt-filled receivers
    - Collector framing details re-sized for a longer “hot” receiver length during operation on-sun, or the specified “cold” receiver length shortened
    - Salt compatible flexible interconnects to link the receiver string to the fixed process piping
    - Physical supports for the HCEs and interconnects outfitted with electrical isolation provisions to separate the piping components from the metal collector framing
    - Attachment provisions on collector structure to support electrical cables and other componentry for the receiver and interconnect heating systems

The Solar Dynamics SunBeam collector was developed under Sunshot Award No. DE-EE0007121 as a next-generation parabolic trough system that is readily reconfigurable for various HTF media, including molten salts. At 8.20m aperture width and 210m maximum collector array length, it is among the largest CSP trough collector systems ever developed. While the SunBeam is fully compatible with conventional HTF media like thermal oils or water, salt-specific provisions like electrical isolation were also incorporated as integral elements during the design development stage to ensure the collector would be “molten salt ready” for future demonstration or deployment scenarios.

For similar reasons, the collector was engineered to be compatible with multiple common HCE sizes, allowing concentration ratio to be varied for the needs of a variety of operational scenarios; ranging from low-temperature hot water process heat applications to high temperature molten salt CSP plants.

This material is based upon work supported by the U.S. Department of Energy’s Office of Energy Efficiency and Renewable Energy (EERE) under the Solar Energy Technology Office Award Number DE-EE0008140.

A key enabling feature is the flatter mirror shape of the large-aperture SunBeam mirror array, which provides higher mirror facet accuracy by reducing errors in the mirror forming process. This improved mirror accuracy is complimented by the SunBeam's rigid steel space frame construction which is both effective and efficient for resisting optical deformations during tracking and when operating in windy conditions. This combination enabled a modest increase in concentration for low-temperature HTF media and supports increasing concentration ratio when needed for high temperature HTF applications.

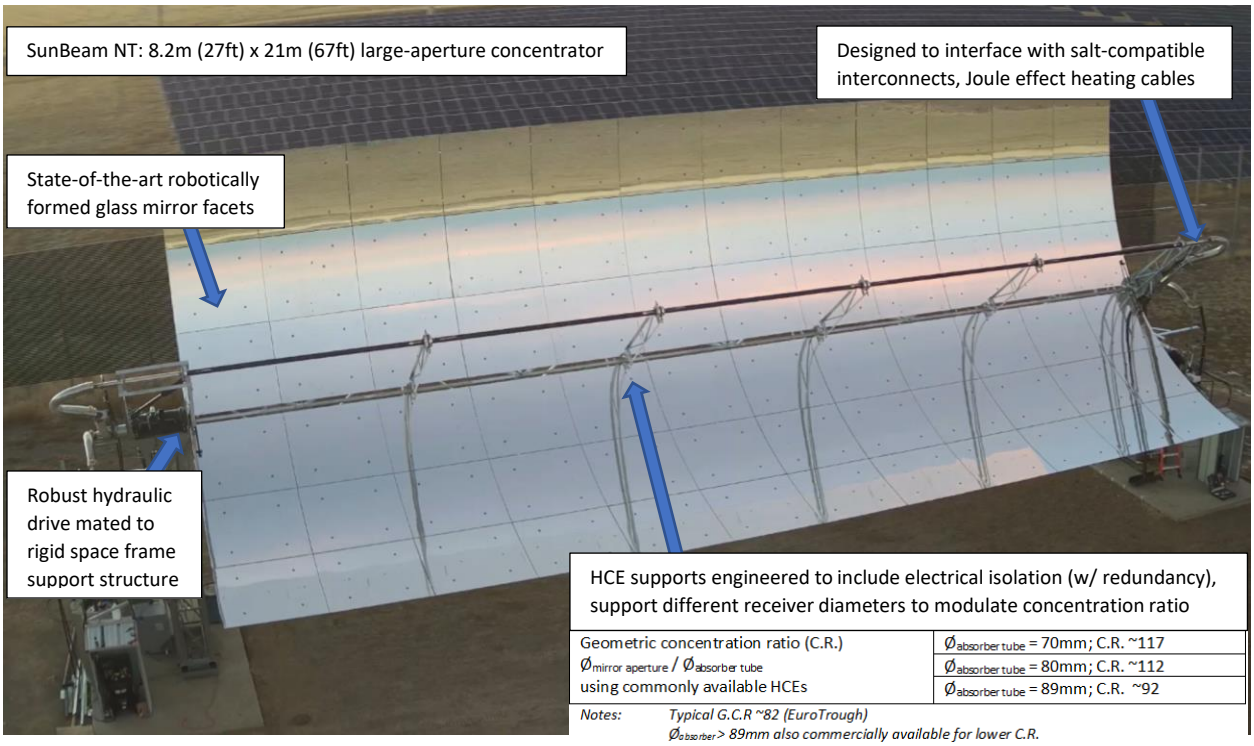

Figure 48. SunBeam™ molten-salt-ready large-aperture trough concentrator

11.4 Collector Loop Configuration

The length of the collector loop is driven by a number of factors.

- Flow hydraulics and heat transfer
- Temperature difference
- Pressure drop
- Land availability

A schematic for the baseline loop is shown below in Figure 49 along with the 1 square mile layout in Figure 50. In this example, the collector at the edge of the solar field by the crossover pipe is shortened to 5 modules to address increased wind loads at the edge of the field.

This material is based upon work supported by the U.S. Department of Energy's Office of Energy Efficiency and Renewable Energy (EERE) under the Solar Energy Technology Office Award Number DE-EE0008140.

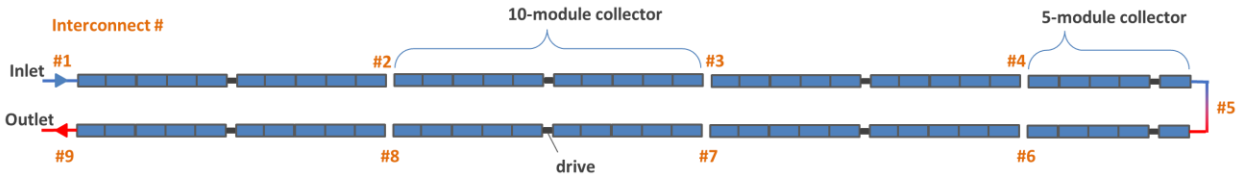

Figure 49. SunBeam™ 70-module loop schematic

11.5 Square mile trough plant

Land in the western U.S. is laid out in sections. A section is a square parcel of land, one mile on side (one square mile or 640 acres of land, or 1609 m x 1609 m). Although not all sections are exactly a square mile, they are generally relatively close. Sections are typically subdivided into smaller parcels, but most county roads and utilities are arranged such that they run between sections rather than through the middle of sections. As a result, there are many square mile sections of land available in the west that have no roads or utilities crossing them. Once you start to look for larger parcels, they often have county roads crossing them. To improve site selection and permitting, we have developed a molten salt trough plant that is designed to fit on a square mile parcel of land including fencing, right of ways, roads, etc. We assume the entire plant fits within the boundaries of the square mile including O&M facilities (offices, warehouse and workshops), and evaporation ponds for wastewater discharge.

It is necessary to have a real site identified in order to develop the design with an accurate cost estimate. We have selected a reference site, 1 mile by 1 mile in size, located in the Harquahala Valley in Arizona. The site has proximity and transmission line right-of-way access to an APS substation. There are multiple sites at this location that could be used for plants. This site could be used to supply power to either Arizona or California transmission substations.

The figure below shows an example of the square mile molten salt trough plant. The plant is laid out with a single east/west header, minimizing the amount of molten salt piping.

This material is based upon work supported by the U.S. Department of Energy's Office of Energy Efficiency and Renewable Energy (EERE) under the Solar Energy Technology Office Award Number DE-EE0008140.

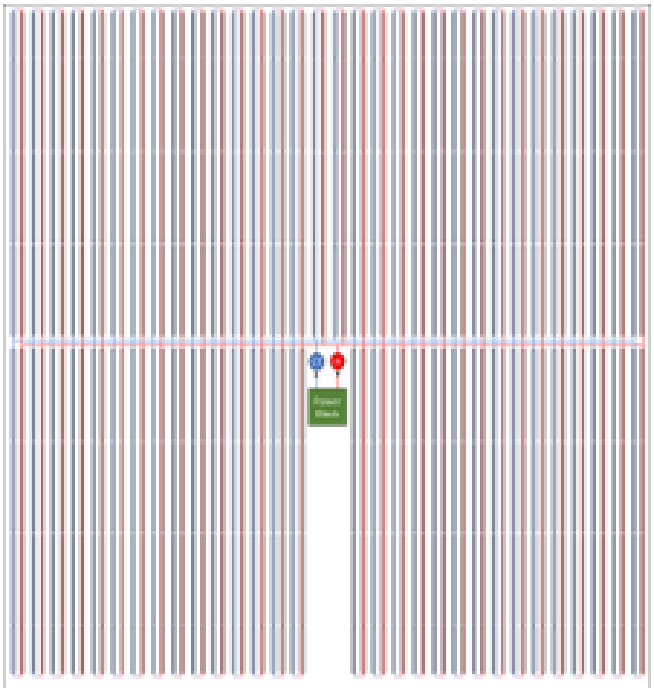

Figure 50. 1mi. (1609m) x 1mi. conceptual solar field layout

11.6 Peaker Plant

Solar Dynamics developed the concept of a dispatchable solar power plant in a prior DOE project (DE-EE0007579). The project developed a molten salt tower plant that was designed to replace the need for new natural gas fired combustion turbines (peakers), for Arizona Public Service (APS). APS had a competitive solicitation where it provided the TOD pricing tiers and values shown in Figure 51. For example, the tier 3 has a multiplier of 9, tier 2 has a multiplier of 3, and tier 1 a multiplier of 1. The zero multiplier during the "No Must Take Energy" tier makes up most of the hours of the year, during this period, no power is accepted by APS. The actual time when the multiplier is $\geqslant$ 1 is 2,618 hr/yr, or ~30% of the time.

This material is based upon work supported by the U.S. Department of Energy's Office of Energy Efficiency and Renewable Energy (EERE) under the Solar Energy Technology Office Award Number DE-EE0008140.

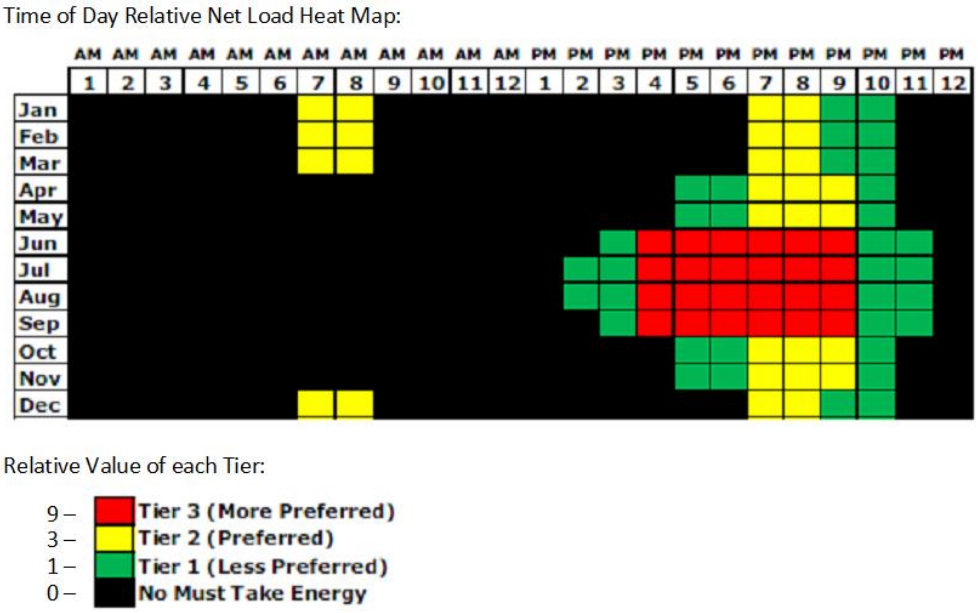

Figure 51: Time of Day Value Heat Map

The peaker plant design was optimized to minimize the bidding prices of power, in essence the tier 1 price (a multiplier of 1).

11.7 Reference Plant Configurations

Solar Dynamics evaluated two plant configurations. The first configuration was a peaker plant that used the square mile plant site and optimized the size of the power cycle, the thermal storage capacity, and the solar field spacing to minimize the LCOE of the plant. The second configuration used the same power cycle size as the peaker plant but removed the square mile land constraint, optimizing the plant for solar field aperture area, row spacing, and TES capacity, again to minimize the LCOE of the plant.

Both the Baseload and Peaker plant configurations have a 200MW (gross) power capacity which was found to be the optimum size for the peaker plant. The Baseload Project has 15 hours of full-load TES and the Peaker Project has 6 hours of TES. When electricity is to be generated, the hot salt is routed to a steam generation system (SGS), which generates steam for use in a high-efficiency regenerative reheat steam Rankine cycle. Both Projects use dry cooling technology for the steam turbine exhaust condensing via an air-cooled condenser (ACC).

11.8 Financial Model Assumptions

The SAM financial model was used for calculating the levelized cost of energy (LCOE). The following lists the main assumptions.

Financial Structure: PPA Single Owner
PPA: 25 years, 1% annual price escalation
Equity IRR: 11%
Debt: 7% interest rate, 18-year debt term, DSCR = 1.3x.
Construction Loan: 24 months, 100% debt.
ITC: 30%, 0% bonus depreciation

This material is based upon work supported by the U.S. Department of Energy's Office of Energy Efficiency and Renewable Energy (EERE) under the Solar Energy Technology Office Award Number DE-EE0008140.

Depreciation: 5-year MACRS 90%, 15-year MACRS 1.5%, 15-year Straight Line 2.5%, 20-year Straight Line 3%
Property Tax: 0%
Sales Tax: 5.0%.
Federal Tax Rate: 21%
State Tax Rate: 7%

11.9 Performance Modeling Optimization

The integrated system model described in Section 10.4 was used to perform the following analyses.

11.9.1 Comparison of Interconnects

The initial optimization utilized cost information from prior project experience and assumptions. The results of the initial optimization for the Peaker configuration were as presented in Figure 52:

Metric	Value
Nominal LCOE	15.0 ¢/kWhr
PPA (Year 1)	3.4 ¢/kWhr (w/ 1% escalator)*
GCR	0.42
# loops	76
SF Aperture Area	840,028 m²
Interconnect type	Flex hose
PB Gross	175 MWe
TES	2600 MWt-hr (6 hrs)
Capacity Factor	23% Annual 92% Summer Peak (Jun-Sept 3-9pm)

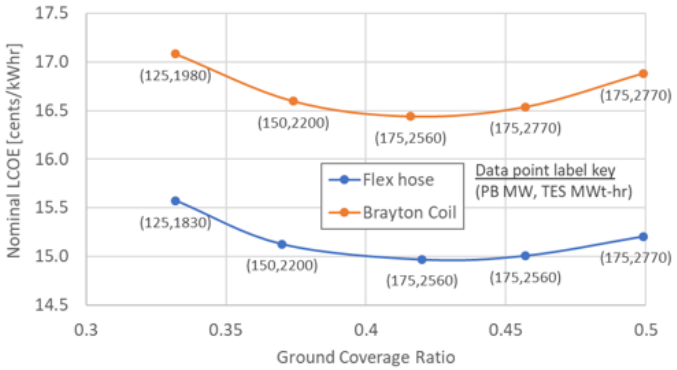

Figure 52. Initial Peaker Plant Optimization

The following were noted in regard to the Flexible Rotary Pipe Coupler versus the flex hose alternatives:

- Flexible Rotary Pipe Coupler suffers from higher heat loss and larger pumping parasitics
  - 1,170% larger annual interconnect heat loss (55.6 GWt-hr total)
  - 45% larger annual pumping parasitics through solar field (3.6 GWe-hr total)
- Flexible Rotary Pipe Coupler design would benefit from 'row' design (no crossover, cold and hot headers at opposite ends of SCAs)
  - Annual SF piping heat loss reduced by 12%, SF pumping parasitics increases by 14% compared to conventional loop design with Flexible Rotary Pipe Coupler
  - LCOE would remain higher than flex hose-based loop

The results of the initial design optimization were used to inform the Conceptual Design Basis discussed in the previous section. Flex hoses are used as the interconnect basis for the remaining analyses.

This material is based upon work supported by the U.S. Department of Energy's Office of Energy Efficiency and Renewable Energy (EERE) under the Solar Energy Technology Office Award Number DE-EE0008140.

11.9.2 Loop Length and Receiver Size

The integrated system model was then used to find the optimum combination of loop length and receiver diameter. A parametric optimization was performed where the figure of merit was the cost/performance of the solar collection system as defined below:

- Figure of Merit: Cost/Performance [$/MWh-th]
- Cost = (Solar Field Cost + HTF System Cost) * (1+EPC and Owner Cost Percentage)
- $$\text{Performance} = \left(\left(\dot{Q}_{abs} - \dot{Q}_{pipe} - \dot{Q}_{int.} - \left(\frac{\dot{Q}_{FP}}{\eta_{HT}*\eta_{PB}} - \dot{Q}_{FP}\right)\right) - \frac{W_{HTFMainPump}}{\eta_{PB}}\right) * DELT$$
    - $\dot{Q}_{abs}$ is thermal energy absorbed by HTF, including heat loss. i.e. Negative in the evening;
    - $\dot{Q}_{pipe}$ is thermal loss of piping system;
    - $\dot{Q}_{int.}$ is thermal loss of interconnects;
    - $\dot{Q}_{FP}$ is electric energy used for freeze protection. $\left(\frac{\dot{Q}_{FP}}{\eta_{HT}*\eta_{PB}} - \dot{Q}_{FP}\right)$ represents performance reduction due to freeze protection. The first term accounts for the electrical power needed to power the heat tracing circuit. The second term accounts for the fact that freeze protection is adding thermal energy to the SF (and this energy can be used for generation, so it is a credit, not a deduction)
    - $W_{HTFMainPump}$ is electric energy consumed by HTF main pumps. Different loop/receiver design consumes different pumping power, so we need to count it.
    - $DELT$ is the simulation time step.

For this study, each SCA contained 10 x 20.9m modules in the interior and 8 x 20.9 m at the exterior of the loop. Loop size was varied from 6-10 SCAs per loop while receiver outer diameter was varied from 80 – 100mm with a constant 2.5 mm wall thickness assumed. All runs were performed with an I-field configuration. Figure 53 presents the final cost/performance results where loop length is grouped by line color, and receiver size is grouped by line type. The smallest 80mm receiver suffers from poor performance dominated by high dumping losses due to pressure constraints. Longer loops benefit from reduced HTF system costs resulting from fewer header sections needed to serve the same solar field aperture. In general, the two most promising configurations are:

- 10 SCA/loop (96 modules/loop) with 100mm OD receivers
- 8 SCA/loop (76 modules/loop) with 90mm OD receivers.

This material is based upon work supported by the U.S. Department of Energy's Office of Energy Efficiency and Renewable Energy (EERE) under the Solar Energy Technology Office Award Number DE-EE0008140.

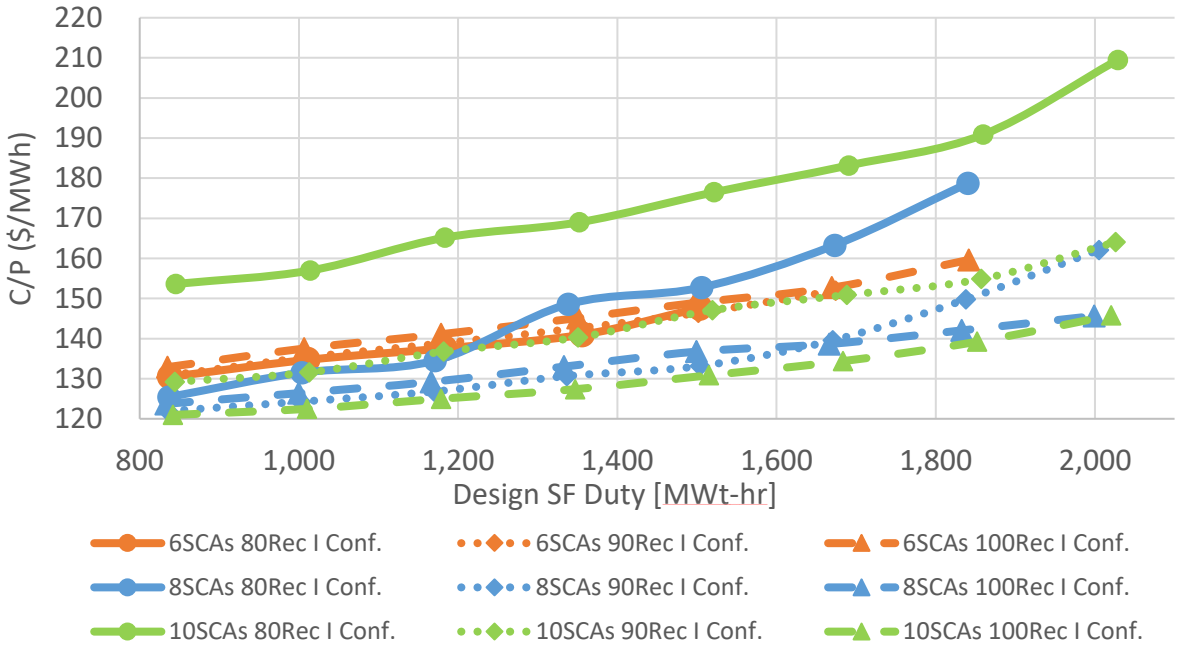

Figure 53 Cost/Performance Results from Initial Loop Sizing

The final loop design was influenced by the above cost/performance results, SunBeam™ collector design constraints, and square mile land constraints. The shorter 8 SCA/loop configuration was chosen to better fit within the square mile field boundary. Lastly, the 90mm receiver was chosen because it had lower cost/performance values when looking at 8 SCA loop lengths.

11.9.3 Final Design Optimization – Peaker Configuration

The Conceptual Design Basis document generated by Advisian was accompanied by updated cost estimates in addition to performance data under variable ambient conditions and operating loads. In parallel, updated information for the costs of the SunBeam™ collector were also received. This updated information was used to re-evaluate the optimizations for the Peaker and Baseload configurations. The final results for the Peaker configuration are shown in Figure 54.

This material is based upon work supported by the U.S. Department of Energy's Office of Energy Efficiency and Renewable Energy (EERE) under the Solar Energy Technology Office Award Number DE-EE0008140.

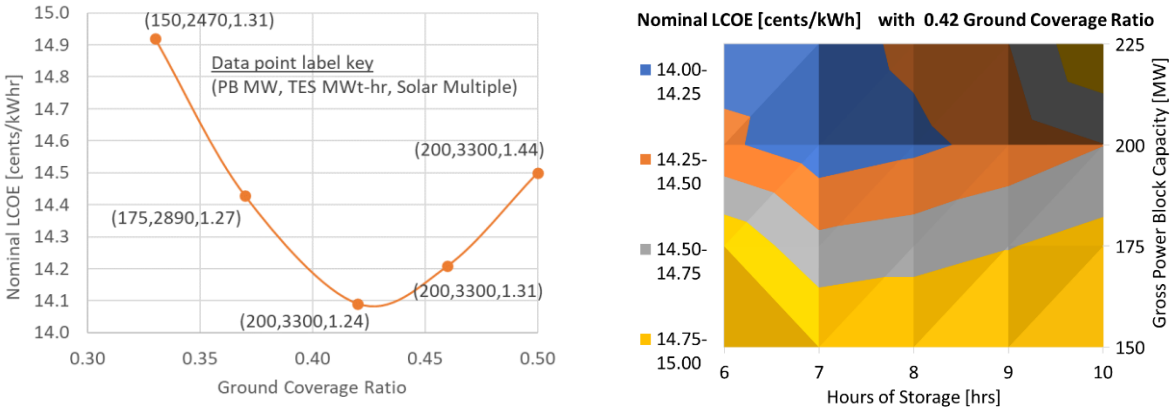

Figure 54. Final Peaker plant: Optimum configurations at varying GCR (left), contour plot of LCOE at optimum 0.42 GCR (right).

Table 9 presents the optimum Peaker plant configuration. The main changes from the initial optimization are an increase in power block and TES size. The reason for this is discussed below.

Table 9 Final Peaker plant optimum design

Initial BP1 Optimum	**Final BP2 Optimum**	**Parameter**
Harquahala Valley, AZ 33.49°N latitude, 113.1°W longitude		Site location
2,903		Annual DNI in TMY weather file [kWhr/m^2]
840,028	867,160	Solar field aperture area [m^2]
76	76	# loops
1.49	1.24	Solar Multiple
19.69	19.69	Row spacing [m]
0.42	0.42	Ground Coverage Ratio (GCR)
6 -- 2,560	7 -- 3,300	TES Capacity [hrs -- MWt-hr]
175	200	PB Gross Capacity [MW]
168	179	Average Net Capacity [MW]
350.1	434.1	Annual Gross Production [GWhr]
321.9	400.4	Annual Net Online Production [GWhr]
20.5	12.4	Annual Net Offline Consumption [GWhr]
14.97	14.09	LCOE (nominal) [cents/kWh]
11.77	11.08	LCOE (real) [cents/kWh]

The following changes were made to the performance model between the initial and final optimizations. Items 1 and 4 below are the largest drivers leading to a larger power block and TES size for the final optimization.

1. Increased collector performance based on final ATLAS reported values

This material is based upon work supported by the U.S. Department of Energy's Office of Energy Efficiency and Renewable Energy (EERE) under the Solar Energy Technology Office Award Number DE-EE0008140.

2. Improved algorithm that calculates the maximum allowable loop flowrate (maximum allowed to not exceed design pressure ratings of piping)
3. Updated power block startup parameters ('Power block startup time' and 'Fraction of thermal power needed for startup') as previous values over-estimated startup energy.
    a. Results in 0.09 for both parameters yielding an average energy of 50 MWt-hr per startup.
4. Initial analysis allowed PB to warm-up in the timestep prior to being dispatched such that full capacity could be provided during priority hours (Figure 51), but this is not possible with 1-hr timesteps and the short startup time above. Final analysis requires power block to warmup and generate within the priority hours only.

The annual production profile of the Peaker is shown in Figure 55. The average net production of the plant is 179 MW. The first hour of operation never reaches this outlet level because of the power block startup time discussed above.

This material is based upon work supported by the U.S. Department of Energy's Office of Energy Efficiency and Renewable Energy (EERE) under the Solar Energy Technology Office Award Number DE-EE0008140.

Table 10 presents the net production and capacity factor each month. The highest priority hours are 3-9 pm in June-September, and during this period the Peaker obtains a 93.9% capacity factor.

Hr↓/ Month→	1	2	3	4	5	6	7	8	9	10	11	12
1	-3	-2	-2	-1	-1	-1	-1	-1	-1	-1	-2	-2
2	-3	-3	-3	-1	-1	-1	-1	-1	-1	-1	-3	-3
3	-4	-3	-3	-1	-1	-1	-1	-1	-1	-1	-3	-3
4	-3	-4	-4	-2	-1	-1	-1	-1	-1	-2	-3	-3
5	-3	-4	-4	-2	-1	-1	-1	-1	-1	-2	-4	-4
6	-4	-4	-4	-3	-2	-1	-1	-1	-1	-2	-4	-4
7	**39**	**125**	**144**	-3	-1	-1	-1	-2	-2	-3	-4	**-4**
8	**-1**	**104**	**151**	-1	-2	-2	-1	-1	-1	-2	-4	**-4**
9	-2	-2	-2	-2	-2	-2	-2	-2	-2	-2	-1	-2
10	-2	-2	-2	-3	-3	-3	-2	-2	-2	-2	-2	-2
11	-2	-2	-2	-3	-3	-3	-2	-2	-2	-2	-2	-1
12	-1	-2	-2	-3	-2	-2	-3	-2	-2	-2	-1	-1
13	-1	-2	-2	-2	-1	-1	-2	-2	-2	-2	-1	-1
14	-1	-1	-2	-1	-1	-1	**155**	**154**	-2	-2	-1	-1
15	-1	-1	-2	-1	-1	**157**	**170**	**169**	**155**	-2	-1	-1
16	-1	-2	-1	-1	-1	**177**	**170**	**168**	**169**	-1	-1	-1
17	-1	-1	-1	**165**	**160**	**178**	**166**	**164**	**171**	**166**	**166**	-1
18	-1	-1	-1	**186**	**181**	**181**	**173**	**164**	**176**	**190**	**172**	-1
19	**162**	**159**	**176**	**185**	**200**	**183**	**164**	**168**	**171**	**180**	**156**	**158**
20	**159**	**169**	**179**	**181**	**187**	**184**	**148**	**157**	**172**	**178**	**152**	**161**
21	**138**	**165**	**168**	**181**	**182**	**179**	**147**	**144**	**172**	**175**	**95**	**141**
22	**112**	**156**	**165**	**178**	**183**	**178**	**147**	**122**	**153**	**167**	**11**	**98**
23	-1	-1	-1	-1	-1	**175**	**133**	**101**	**122**	-1	-2	-2
24	-2	-2	-2	-1	-1	-1	-1	-1	-1	-1	-2	-2

Figure 55 Final Peaker optimum: 12x24 of average net generation [MW], hours outlined where time of delivery factors > 0

This material is based upon work supported by the U.S. Department of Energy's Office of Energy Efficiency and Renewable Energy (EERE) under the Solar Energy Technology Office Award Number DE-EE0008140.

Table 10 Final Peaker optimum: net production and capacity factor

Month [--]		1	2	3	4	5	6	7	8	9	10	11	12	annual
Net Production [GWe-hr]		17.7	23.5	29.2	31.3	33.0	47.0	48.1	46.1	43.2	31.8	21.3	15.9	388.0
Net Capacity Factor [--]	All Hours	13.3	19.5	21.9	24.2	24.7	36.4	36.0	34.6	33.4	23.8	16.5	11.9	24.7
	TOD Tier 2&3 Hrs	50.1	77.6	90.6	101.6	105.7	100.5	89.9	89.6	95.8	99.1	74.8	43.4	85.4

11.9.3.1 Performance and Cost Compared to Oil HTF Trough

The following performance and cost metrics include a comparison to a Therminol oil based HTF plant. The oil trough plant has the same overall size of solar field, TES, and power block, but with the following changes to reflect the change to Therminol HTF and its lower max operating temperature:

- 391°C solar field outlet temperature
- 4 SCA per loop
- 8 modules per SCA
- 40% power block gross design efficiency
- Standard oil-trough system configuration with coupled collection and generation flow loops (i.e. oil-steam HX in steam generator)

Table 11 presents the cost breakdown, overall production, and LCOE for both plants. The following observations are made:

- Increase in TES unit costs for an oil trough dominates the direct cost increase for an oil trough
- Annual generation for MS trough is higher primarily because of higher PB efficiency and secondarily due to HTF pumping parasitics being lower for the MS trough
- MS as the HTF has a large impact in LCOE as expected with a 36 % (8.08 cents/kWh) reduction in nominal LCOE.

Table 11. Cost summary of final optimized Peaker configuration

	MS Trough		Oil Trough	
Direct Capital Cost Summary	**Totals**	**Unit Cost**	**Totals**	**Unit Cost**
Site Improvements	$11,435,000	$13	$11,435,000	$13
Solar Field	$107,295,838	$124	$104,528,640	$120
HTF System (SF Piping)	$43,929,929	$51	$82,112,626	$94
Thermal Energy Storage	$73,907,577	$22	$254,389,701	$73
Power Plant	$222,137,295	$1,111	$196,696,848	$983
Contingency	$45,870,564	10%	$64,916,281	10%
Total Direct Costs	**$504,576,202**		**$714,079,096**	

This material is based upon work supported by the U.S. Department of Energy's Office of Energy Efficiency and Renewable Energy (EERE) under the Solar Energy Technology Office Award Number DE-EE0008140.

Indirect Capital Cost Summary				
EPC and Owner Costs	$61,558,297	12.2%	$87,244,282	12.2%
Land + Permitting	$23,836,301	$37,244	$25,515,448	$39,868
DC's Sales Tax	$19,154,423	76% of direct costs sales tax applied	$32,200,938	90% of direct costs sales tax applied
Total Installed Cost	**$609,125,222**		**$859,039,764**	
O&M Summary				
Fixed Cost by Capacity [$/kW-yr]		$44.9		$44.0
Variable Cost by Generation [$/MWh]		$0.15		$0.16

Annual Generation [MW-hr]	388,043	337,778
LCOE nominal [cents/kWh]	14.09	22.17
LCOE real [cents/kWh]	11.08	17.6

11.9.4 Final Design Optimization – Baseload Configuration

A baseload plant was optimized using the 200 MW gross power block size from the optimum Peaker design. The optimization sought to find the minimum LCOE plant by varying solar field size (i.e. solar multiple), collector row spacing (i.e. GCR), and storage size. The baseload was not constrained to fit within a square mile parcel. The final results for the Baseload configuration are shown in Figure 56.

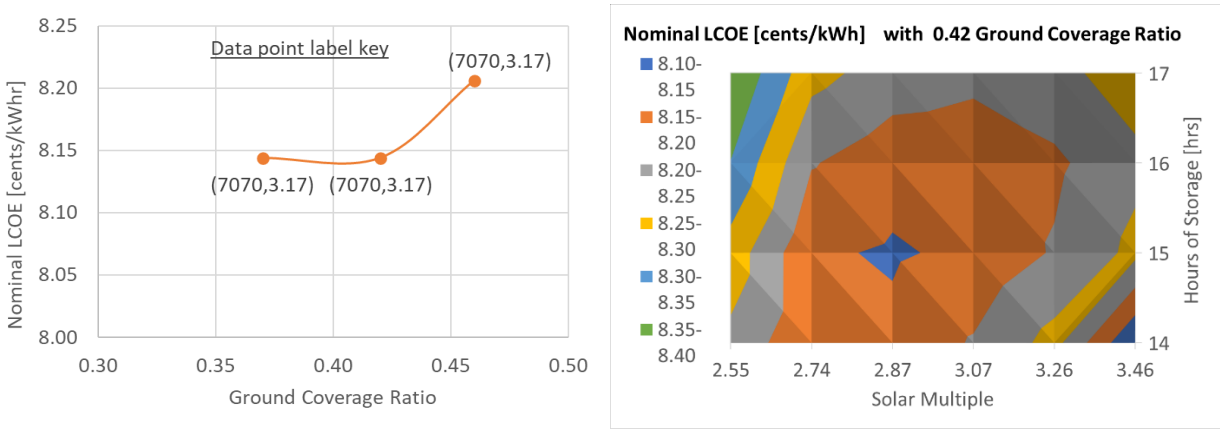

Figure 56. Final Baseload plant: Optimum configurations at varying GCR (left), contour plot of LCOE at optimum 0.42 GCR (right).

Table 12 presents the optimum Baseload plant configuration.

This material is based upon work supported by the U.S. Department of Energy's Office of Energy Efficiency and Renewable Energy (EERE) under the Solar Energy Technology Office Award Number DE-EE0008140.

Table 12 Final Baseload plant optimum design

Final BP2 Optimum	**Parameter**
Harquahala Valley, AZ 33.49°N latitude, 113.1°W longitude	Site location
2,903	Annual DNI in TMY weather file [kWhr/m^2]
1,447	Project land area [acre]
2,008,160	Solar field aperture area [m^2]
176	# loops
3.17	Solar Multiple
19.69	Row spacing [m]
0.42	Ground Coverage Ratio (GCR)
15 – 7,070	TES Capacity [hrs -- MWt-hr]
200	PB Gross Capacity [MW]
182	Average Net Capacity [MW]
1,203.1	Annual Gross Production [GWhr]
1,103.8	Annual Net Online Production [GWhr]
8.9	Annual Net Offline Consumption [GWhr]
8.14	LCOE (nominal) [cents/kWh]
6.41	LCOE (real) [cents/kWh]

The annual production profile of the Baseload plant is shown in Figure 55, and

This material is based upon work supported by the U.S. Department of Energy's Office of Energy Efficiency and Renewable Energy (EERE) under the Solar Energy Technology Office Award Number DE-EE0008140.

Table 10 presents the net production and capacity factor each month.

Hr↓/ Month→	1	2	3	4	5	6	7	8	9	10	11	12
1	-3	31	140	163	179	183	156	156	172	68	-3	-4
2	-4	13	130	160	180	184	156	157	162	20	-3	-5
3	-5	8	107	157	179	185	151	145	152	16	-4	-6
4	-6	-4	96	158	167	185	148	123	139	5	-5	-7
5	-7	-5	59	158	162	186	141	112	119	-2	-6	-7
6	-7	-6	41	152	153	186	134	107	72	-3	-7	-8
7	-7	-7	19	148	149	181	128	94	34	-4	-8	-9
8	-8	-7	3	49	170	185	124	22	-1	-3	-8	-10
9	-3	-3	74	175	182	184	159	132	154	74	-2	-2
10	59	128	152	182	181	173	167	148	171	172	132	90
11	136	160	174	174	175	175	170	158	168	183	162	147
12	147	163	179	176	175	172	166	164	171	184	165	158
13	161	166	164	180	177	172	162	171	165	179	169	159
14	157	163	168	171	171	172	163	171	165	175	162	167
15	162	162	168	176	174	177	163	171	165	175	173	157
16	159	163	171	179	175	177	168	167	170	178	165	149
17	154	169	172	173	184	178	174	167	172	182	176	159
18	124	186	175	174	184	181	174	174	185	181	154	114
19	116	155	164	174	214	186	182	185	174	171	150	56
20	81	143	160	173	186	184	168	159	172	172	109	-1
21	47	132	158	174	181	185	164	160	173	170	71	-1
22	16	123	159	175	182	180	165	160	174	164	18	-2
23	0	105	153	172	183	181	156	161	174	155	3	-2
24	-2	62	145	166	180	182	149	162	175	105	-2	-3

Figure 57 Final Baseload optimum: 12x24 of average net generation [MW]

Table 13 Final Baseload optimum: net production and capacity factor

Month [--]	1	2	3	4	5	6	7	8	9	10	11	12	annual
Net Production [GWe-hr]	45.5	61.6	97.1	118.2	131.5	130.0	117.4	109.3	107.2	84.2	52.8	40.0	1094.9
Net Capacity Factor [--]	33.7	50.4	71.8	90.4	97.3	99.4	86.9	80.9	82.0	62.3	40.4	29.6	68.8

This material is based upon work supported by the U.S. Department of Energy's Office of Energy Efficiency and Renewable Energy (EERE) under the Solar Energy Technology Office Award Number DE-EE0008140.

12 Project Conclusions

12.1 Significant Results and Documents

12.1.1 Reports and Technical Documentation

The following reports were prepared by the project:

- RPPR December 31, 2017
- Materials for DOE Solar Energy Technology Office Portfolio Review Meeting in Feb. 2018, three-page summary and one poster
- RPPR March 31, 2018
- RPPR June 30, 2018
- RPPR September 30, 2018
- “SMART Trough Interconnection Performance Study,” Brayton Energy, December 19, 2018
- RPPR December 31, 2018
- RPPR March 31, 2019
- RPPR June 30, 2019
- RPPR September 30, 2019
- Presentation at SolarPACES 2019 by Luca Imponenti, Daegu South Korea, “CFD modeling of nitrate salts in a receiver tube for freeze recovery,” October 2, 2019
- Presentation at SolarPACES 2019 by Ryan Shininger, Daegu South Korea, “Flexible Hose Interconnect Testing for Parabolic Troughs with Nitrate Salt,” October 4, 2019
- RPPR December 31, 2019
- RPPR March 31, 2020
- RPPR June 30, 2020
- “Mobile Impedance Heating System Design Basis, SMART Molten Salt Trough Project,” Advisian Worley Group, June 30, 2020
- "Conceptual Design Basis, SMART Molten Salt Trough Project," Advisian Worley Group, July 16, 2020
- Poster & Paper submitted for SolarPaces Conference 2020, “Development and Testing of a Solar Flux Heating Freeze Recovery System for Molten Salt Parabolic Troughs,” Leading author: Luca Imponenti, September 29, 2020
- RPPR September 30, 2020
- RPPR December 31, 2020
- RPPR March 31, 2021
- RPPR June 30, 2021

12.1.2 Publications

The following dissemination of result were made:

- R. Shininger, K. Kattke, M. Anderson, F. Vives, M. Saur, M. Boyd, and H. Price, "Flexible Hose Interconnect Testing for Parabolic Troughs with Nitrate Salt," AIP Conference Proceedings, vol 2303, no. 1, 2020, doi: 10.1063/5.0029000.

This material is based upon work supported by the U.S. Department of Energy’s Office of Energy Efficiency and Renewable Energy (EERE) under the Solar Energy Technology Office Award Number DE-EE0008140.

- L. Imponenti, R. Shininger, K. Gawlik, H. Price, and G. Zhu, "Controllable Solar Flux Heating for Freeze Recovery in Molten Salt Parabolic Trough Collectors," J. Energy Resources Tech., vol. 142, no. 12, 2020, doi: 10.1115/1.4047303.
- S. Kraemer, "Promising Test Results for Molten Salts in Trough CSP," CSP News & Analysis, 2020
- L. Imponenti, J. C. Herruzo, R. Shininger, H. Price and J. Valverde "Development and Testing of a Solar Flux Heating Freeze Recovery System for Molten Salt Parabolic Troughs," AIP Conference Proceedings, in press

12.2 Conclusions

The use of molten salt as the HTF in CSP plants has the potential to disruptively reduce the cost of flexible renewable energy. This project focused on implementing a molten salt HTF in parabolic trough CSP plants, the most commercially mature CSP technology. The interconnect technology and freeze recovery of the solar fields are considered the biggest challenges preventing commercialization of molten salt parabolic troughs. This project demonstrated concepts to address the perceived risks of freeze events in the solar field and lower the costs of freeze protection systems. The project accomplishments are summarized as follows:

- A flexible hose interconnect design was lab tested at operating temperature and pressure with solar salt, surpassing the equivalent of 30 years of mechanical cycling without leaking.
- A novel "track-through" strategy to augment freeze protection and freeze recovery using concentrated solar flux was modeled and tested, presenting an opportunity for improved reliability and reduced costs.
- The conceptual design for a mobile Joule heating system was generated, presenting the possibility to displace a fixed heating system estimated to cost \$80/m^2 with one that costs less than \$10/m^2.
- Working with NREL, we adapted the NREL System Advisor Model to simulate a molten-salt trough plant more accurately. While valuable, the improvements have notable limitations and would benefit from future work:
    - The updates have not been added to SAM's user interface. It would be very challenging for an unknowing user to make use of the added molten salt trough capabilities.
    - Documentation for the use of these molten salt trough updates has not been generated.
- Working with Advisian, we developed an updated cost model that works with SAM to allow accurate comparisons between oil and molten salt trough plant configurations.
- Plant performance and costs models for both molten salt trough plants and conventional oil plants were updated. Optimal configurations were identified, both for a Baseload power plant (with high capacity factor) and for a "Peaker" configuration (lower capacity factor, storing and delivering energy only at the highest demand periods).

The cost advantages molten salt troughs is compelling, presenting LCOE reductions on the order of 35-40% relative to conventional oil troughs. The following factors contribute to the cost advantages of molten salt compared to oil HTF:

- Increased Rankine cycle efficiency
- 2.5X greater energy density in the salt results in multiple opportunities for savings

This material is based upon work supported by the U.S. Department of Energy's Office of Energy Efficiency and Renewable Energy (EERE) under the Solar Energy Technology Office Award Number DE-EE0008140.

    - Reduced TES system volume by approximately 60% for the same amount of stored energy
    - Smaller header piping and less HTF in the solar field
    - Reduced parasitic power required for pumping
    - Single east/west header instead of two, eliminating the need for north/south headers
- Solar salt is less expensive than oil HTF
- Elimination of 1 heat exchanger due to two fluid system (salt & steam) instead of three (oil, salt, & steam)
    - Energy savings from the elimination of the associated approach temperatures

Other factors add costs to a molten salt trough plant relative to conventional oil HTF (although they are greatly outweighed by the cost advantages listed above):

- Hot portions of the piping must be stainless instead of carbon steel
- The hot tank must be stainless steel
- Portions of the steam generator must be stainless instead of carbon steel
- Interconnects are more expensive than options available for oil troughs (although conventional oil trough solutions have not proven to be fully reliable).

Despite the compelling cost advantages, the potential risks associated with freeze events remains a barrier to the finance-ability and commercial deployment due to limited technology demonstration. The following future efforts are recommended:

- A design basis document should be generated for nitrate molten salt systems in CSP projects covering topics including the heat trace system design and redundancy, storage tank foundation design, Joule heating system design and implementation, etc.
- A full-scale pilot collector loop should be constructed and operated. A collector loop represents the fundamental building block of a commercial solar field, so if one can be demonstrated to operate reliably, it follows that an entire solar field can accomplish the same.
    - Although other demonstration loops have been constructed, knowledge sharing has been limited.
    - Any company considering the deployment of molten salt trough plants should gain first hand practical experience by way of fielding a collector test loop.
- A detailed design of the mobile impedance heating system should be completed such that it can be constructed and demonstrated on the pilot collector loop.
- The flex hose interconnect requires some design modification to make for more evening Joule heating and more even thermal losses through its differing components. The interconnect needs to be tested with daily swings of temperature and pressure in addition to the mechanical cycling.

This material is based upon work supported by the U.S. Department of Energy's Office of Energy Efficiency and Renewable Energy (EERE) under the Solar Energy Technology Office Award Number DE-EE0008140.

References

[1] "EERE 123: Technology Readiness Levels".

[2] K. &. Associates, "Engineering & Evaluation of a Molten Salt HTF in a Parabolic Trough Solar Field," NREL Contract No. ANN-30441-04, Final Report, 2002.

[3] Fabrizi, "Trough Molten Salt HTF Field Test Experience Experimental remarks on behaviour during operation and thermal fluid dynamics in transition states of molten salt mixtures," NREL Parabolic Trough Workshop, Golden, Colorado, March 2007.

[4] D. Grogan, "Development of Molten-Salt Heat Transfer Fluid Technology for Parabolic Trough Solar Power Plants," Abengoa Solar, DE-FC36-08GO18038, 2013.

[5] G. Kolb, C. Ho, B. Iverson, T. Moss and N. Siegel, "Freeze-thaw tests on trough receivers employing a molten salt working fluid," in *Proceedings of ASME Energy Sustainability*, 2010.

[6] W. Gaggioli, F. Fabrizi, L. Rinaldi and P. Di Ascenzi, "Experimental tests about the cooling/freezing of the molten salts in the receiver tubes of a solar power plant with parabolic trough," in *AIP Conference Proceedings*, 2017.

[7] C. Prieto, A. Rodríguez-Sánchez, F. J. Ruiz-Cabañas and L. F. Cabeza, "Feasibility study of freeze recovery options in parabolic trough collector plants working with molten salt as heat transfer fluid," *Energies,* vol. 12, no. 12, pp. 1-20, 2019.

[8] D. Kearney, B. Kelly and U. e. a. Herrmann, "Engineering aspects of a molten salt heat transfer fluid in a trough solar field," *Energy,* vol. 29, no. 5-6, pp. 861-870, 2004.

[9] W. Caruso, "Flexible Rotary Pipe Interconnection, DE-SC0011965," 2018.

[10] P. Marcotte, "Final Technical Report, DE-EE0007121: ATLAS: Advance Trough with Low-cost System Architecture," https://www.energy.gov/eere/solar/project-profile-abengoa-solar-llc-atlas, 2021.

[11] I. I. E. &. E. Co., "Impedance Heating Systems," St. Louis, MO, 2004.

[12] L. Imponenti, R. Shininger, K. Gawlik, H. Price and G. Zhu, "Controllable Solar Flux Heating for Freeze Recovery in Molten Salt Parabolic Trough Collectors," *Journal of Energy Resources Technology,* vol. 142, no. 12, 2020.

[13] J. C. H. R. S. H. P. a. J. V. L. Imponenti, "Development and Testing of a Solar Flux Heating Freeze Recovery System for Molten Salt Parabolic Troughs," in *AIP Conference Proceedings*, in press.

This material is based upon work supported by the U.S. Department of Energy's Office of Energy Efficiency and Renewable Energy (EERE) under the Solar Energy Technology Office Award Number DE-EE0008140.

[14] B. D. Iverson, S. T. Broome, A. M. Kruizenga and J. G. Cordaro, "Thermal and mechanical properties of nitrate thermal storage salts in the solid-phase," *Solar Energy,* vol. 86, no. 10, pp. 2897-2911, 2012.

[15] ASME, "Boiler and Pressure Vessel Code," *BPVC.II.D.M-2017,* 2017.

[16] R. Forristall, "Heat Transfer Analysis and Modeling of a Parabolic Trough Solar Receiver Implemented in Engineering Equation Solver," NREL/TP-550-34169, 2003.

[17] F. Burkholder and C. Kutscher, "Heat loss testing of Schott's 2008 PTR70 parabolic trough receiver," NREL/TP-550-45633, 2009.

[18] W. G. Advisian, "Conceptual Design Basis, SMART Molten Salt Trough Project," 2020.

This material is based upon work supported by the U.S. Department of Energy's Office of Energy Efficiency and Renewable Energy (EERE) under the Solar Energy Technology Office Award Number DE-EE0008140.